THE PENNSYLVANIA STATE UNIVERSITY
SCHREYER HONORS COLLEGE

DEPARTMENT OF MECHANICAL ENGINEERING

Development of a Scaled Experimental Testbed for Hybrid Electric Aircraft

CARLY DUNFORD
SPRING 2023

A thesis
submitted in partial fulfillment
of the requirements
for a baccalaureate degree
in Mechanical Engineering
with honors in Mechanical Engineering

Reviewed and approved* by the following:

Dr. Herschel Pangborn
Assistant Professor of Mechanical Engineering
Thesis Supervisor

Dr. Margaret Byron
Assistant Professor of Mechanical Engineering
Honors Advisor

* Electronic approvals are on file.

ABSTRACT

Hybrid electric aircraft are increasingly a focus of research and development in the aerospace industry. These aircraft have the potential to be more sustainable than traditional aircraft and offer other possible benefits. There are many ways to create a powertrain for a hybrid electric aircraft, and choosing which configuration is the best for a given set of flight requirements can be challenging. Different propulsion configurations provide various advantages to the aircraft. There is currently no comprehensive way to compare all the configurations due to the variables in each aircraft body shape, wing length, maximum takeoff weight, mission requirements, and many other factors. This work aims to develop a testbed to analyze many different hybrid electric aircraft propulsion configurations without rearranging components. The eventual goal is to develop a rapidly reconfigurable testbed to represent different candidate powertrain designs. To start this design process, Simulink was used to determine the type and size of parts needed for the testbed. By running simulations of the powertrains, the ideal part parameters were determined. After these parts were ordered, a testbed structure was created to test the functionality and interaction of the parts safely. Multiple testbed cage and motor mount designs were created and analyzed using SolidWorks. Final testbed layouts were selected and created. Using the final testbed motor mounts, two motors were coupled together as a motor and dynamometer pair and then run at a low speed to determine the interaction between the motors and develop a method to ensure the motors are precisely aligned. Once the testbed cage is completed, future students will work to transform the testbed to become reconfigurable.

TABLE OF CONTENTS

LIST OF FIGURES iii

LIST OF TABLES iv

ACKNOWLEDGEMENTS v

Chapter 1 Introduction 1

- Motivation 2
- Goals and Objectives 4

Chapter 2 Literature Review 5

- Optimization Studies of Potential Full-Scale Vehicles 5
- Simulation of Testbeds 7
- Implementation of Physical Testbeds 8
- Airborne Testbeds 10

Chapter 3 Dynamic Model of the Propulsion Configuration 13

- Component Block Models 13
- Final Simulink Model 16
- Adding the Torque Profile to the Final Model 21

Chapter 4 Creating a Physical Testbed 25

- Selecting Parts 25
- Design of Mounts 27
- Prototype of Mounts 29
- Assembly of Mounts 30
- Design of Testbed 32

Chapter 5 Testing the Testbed 36

- Testing the Motors 36
- Creating a PWM Signal 37
- Running the Speed Controller 39
- Simulating the Engine 40
- Connecting Simulink to Arduino 41
- Connecting Simulink to the ESC 42

Chapter 6 Conclusion and Future Work 45

- Summary of Work 45
- Ideas for Future Work 46

Appendix A Datasheets for Parts in Testbed 48

Appendix B Arduino Code 49

Appendix C Engineering Drawings of Testbed Layout 50

BIBLIOGRAPHY 52

LIST OF FIGURES

Figure 1. NASA Electric Aircraft Testbed (NEAT) Layout [1], work of the U.S. Government; public use permitted 2

Figure 2. Spacecraft Control Testbed Layout, reprinted from [2], with permission from Open Access Creative Commons CC BY License 2

Figure 3. Hybrid Aircraft Propulsion Configurations, reprinted from [6] with permission 3

Figure 4: Examples of Blocks in Modeling Toolbox 13

Figure 5: Inside the Motor Block from Modeling Toolbox 14

Figure 6: Block Diagram of Simulink Model 15

Figure 7: Y to Delta Conversion 15

Figure 8: Simulink Model for Motor Testing 16

Figure 9: Fixed Wing Aircraft Torque Profile 17

Figure 10: Simulink Model with Motor and Inverter 18

Figure 11: Motor Current and Speed vs. Time 18

Figure 12: Adding the Generator 20

Figure 13: Motor Speed vs. Time of Model with Generator and PID Control 20

Figure 14: Series Hybrid Electric Model in Simulink 22

Figure 15: Battery State of Charge vs. Time for Given Torque Profile 23

Figure 16: Neu Motor 6515 26

Figure 17: First Motor Mount Design 27

Figure 18: Second Motor Mount Design 28

Figure 19: First Motor Mount Prototype 30

Figure 20: Adjusted Motor Mount Prototype 31

Figure 21: Aluminum Motor Mounts 31

Figure 22: Motor on Aluminum Motor Mount 32

Figure 23: Motor Mount Pair Layout Options (Top View) 33

Figure 24: Testbed Design Isometric View 34

Figure 25: PWM Signal Testing Circuit 38

Figure 26: Range of PWM Signals Sent to Motor 39

Figure 27: Hybrid Propulsion Configuration Model, Turbo shaft block from [40] 40

Figure 28: Simulink to Arduino Motor Control Setup 42

Figure 29: Assembled Dual Motor Mount with Coupling Attached 43

Figure 30: Output Signal of Coupled Motor 44

Figure 31: Designed Testbed Implementation on a Larger Scale 46

Figure 32: Testbed Cage Dimensions 50

Figure 33: Dual Motor Mount Dimensions 51

LIST OF TABLES

Table 1. Simulated Motor Parameters 24

Table 2: Motor Parameters Used as Reference..... 24

Table 3: Neu Motor 6515 Parameters..... 25

Table 4: Testbed Material List..... 35

Table 5: Testbed Part List and Datasheets..... 48

ACKNOWLEDGEMENTS

First, I would like to thank Dr. Pangborn for all his support and guidance throughout this project. Dr. Pangborn always made himself available to guide and advise me and was always available to answer questions. This project has been an enjoyable learning experience for me. I have also enjoyed my time being part of the PAC Lab group, where I always felt welcomed. I would like to thank the students in PAC Lab, as many of them also helped me with this project.

Dr. Hall, Aaron Vanlandingham, and Alvin Binu from the Aerospace Engineering Department provided great help and collaboration throughout the project. The final version of the testbed will be built in Dr. Hall's laboratory. Dr. Hall, Aaron, and Alvin provided expertise in aircraft performance, and I am grateful for their help in developing this testbed.

I would like to thank the Schreyer Honors College for the funding and support throughout this process and for the unique experiences the college has provided during my time at Penn State. Last but certainly not least, I would like to thank my parents for all their encouragement and support throughout my academic career. I would not have been able to do any of this without them.

Chapter 1

Introduction

This research thesis, conducted with the Pangborn Advanced Controls Lab, will study how to create a scaled testbed for hybrid aircraft that eventually can be reconfigurable to emulate many different propulsion configurations. Propulsion configurations or architectures reflect different ways to produce power and thrust for the aircraft. For example, most commercial aircraft use gas turbine engines that combust fuel to produce thrust and power. Testbeds can be constructed with the critical aircraft components to be studied to research propulsion configurations in a laboratory environment. Without the aircraft's frame, these components may include power electronics, data acquisition and communications equipment, thermal components, and propulsion components. Testbeds can come in many different sizes. An example of a large-scale NASA testbed is shown in Figure 1, while an example of a small-scale spacecraft testbed is shown in Figure 2 for comparison.

The testbed in this thesis will consist of key aircraft powertrain components coupled together to test the equipment's functionality and control integration, with hardware and software as close to real aircraft systems as possible but at a smaller scale to facilitate ease of implementation. Some systems may be simulated where hardware is unavailable or feasible to implement (e.g., gas turbine engines) via “hardware-in-the-loop” testing. This testbed will address electric propulsion configurations powered by batteries, as well as hybrid propulsion configurations that include different combinations of conventional and electrical drive systems.

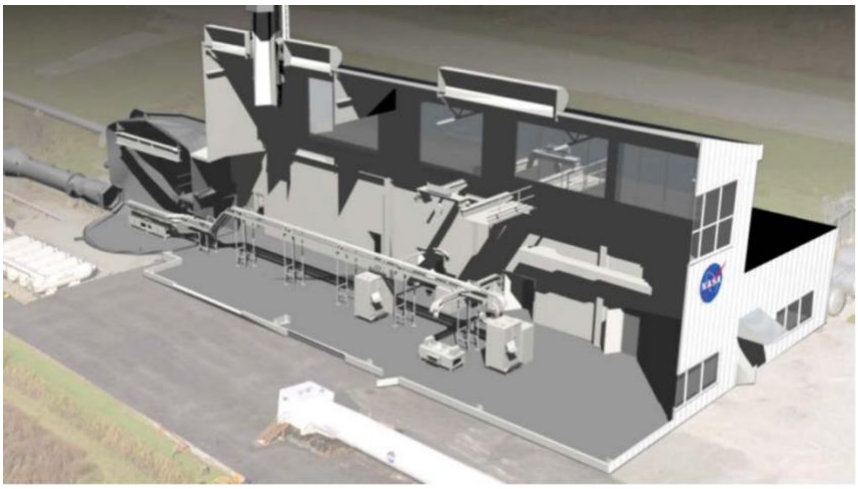

Figure 1. NASA Electric Aircraft Testbed (NEAT) Layout [1], work of the U.S. Government; public use permitted

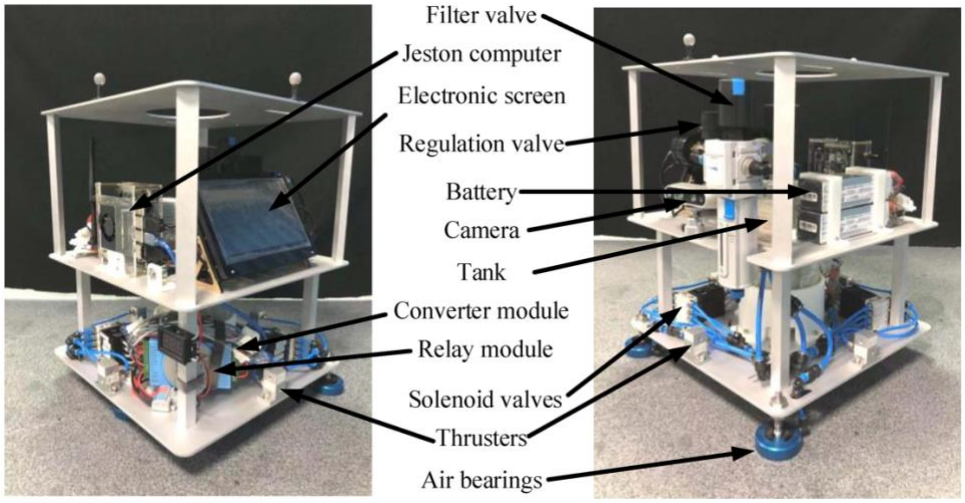

Figure 2. Spacecraft Control Testbed Layout, reprinted from [2], with permission from Open Access Creative Commons CC BY License

Motivation

This research aims to improve aircraft technology to make aviation more efficient, sustainable, and cost-effective. Electric aircraft are rising in interest, but batteries are not yet dense enough in energy or power to handle long-range missions [3]. Hybrid aircraft may utilize some

benefits of electrification without relying solely on a battery for energy storage. For military applications, small hybrid unmanned aerial vehicles (UAVs) can be used for stealth missions, periodically turning off their engine to run more quietly on battery power [4]. Creating a reconfigurable testbed allows one to test multiple hybrid configurations, like those shown in Figure 3, for flight profiles and missions. Figure 3 shows examples of six hybrid electric aircraft propulsion configurations, including how each component, such as the batteries or motors, is connected in each scenario. These studies can positively impact current and future electrified aircraft in development. Hybrid electric aircraft powertrains include more complicated integration with other aircraft components because multiple power sources need to work together and communicate [5].

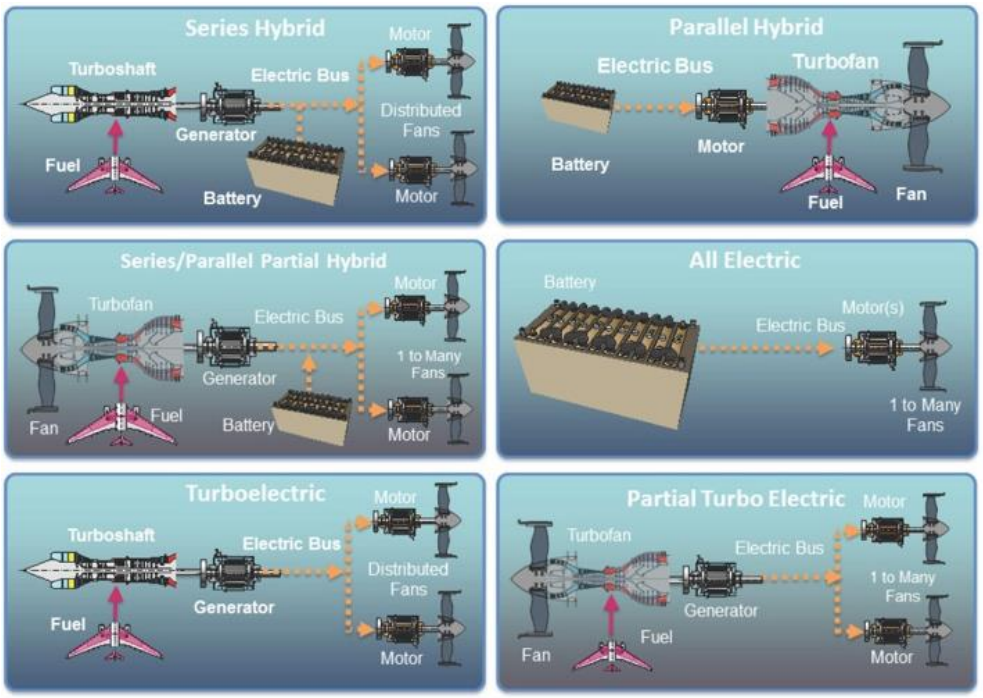

Figure 3. Hybrid Aircraft Propulsion Configurations, reprinted from [6] with permission

Goals and Objectives

This research thesis aims to study how a small-scale hybrid electric aircraft testbed can be developed. The goal is to create a platform that can be developed to allow one to switch configurations without substantially moving or rewiring any part of the testbed. First, a dynamic simulation of the hybrid electric testbed will be created in MATLAB/Simulink. The simulation will evaluate possible sizes and specifications for each component. The results of the simulation studies will be used to determine the ideal size and specifications of hardware components to purchase for the small-scale experimental system. After components are selected, the small-scale testbed will be assembled. These objectives will be pursued in collaboration with members of Dr. David Hall's research group in the Penn State Department of Aerospace Engineering. Once the testbed is complete, it will compare performance across different control strategies, mission profiles, and powertrain configurations.

Chapter 2

Literature Review

Many companies and research agencies are developing hybrid aircraft. Due to the significant push for further electrification in aviation, there are many papers published about the design, simulation, and testing of electrified aircraft energy systems. This may include one or multiple of propulsion, power, and thermal management subsystems [7] and avionics software [8]. Building a physical testbed includes testing parts for large aircraft and spacecraft [9]. These testbeds can analyze the desired vehicle's software, component performance, powertrains, or energy sources [10]. The existing testbeds and simulations of vehicles documented in this literature provide the bases on which this thesis seeks to contribute new capabilities.

Optimization Studies of Potential Full-Scale Vehicles

When starting the design of a vehicle, it is important to test multiple design layouts to determine which best optimizes the desired mission. Brelje and Martins published their design approaches for electric, hybrid, and turboelectric fixed-wing aircraft [11]. Their design approach consisted of identifying the possible electrified propulsion configurations and analyzing the benefits and drawbacks of each configuration. Tran et al. designed a hybrid electric vehicle powertrain that optimizes performance [12]. To determine the best configuration, the team simulated multiple powertrains under their desired conditions. It was concluded that a hybrid powertrain with a combination of series and parallel connections was ideal.

For the research done in this thesis, a similar approach to those described previously was taken to design the testbed. First, an electric aircraft powertrain was developed in Simulink to test

different component parameters. Using the Simulink model, we could determine what size components to order for the physical testbed. The components in the testbed were designed with modularity in mind for the future. Turboshaft engines in different connections, i.e., parallel vs. series, can be emulated in the electric powertrain later.

Some full-scale vehicle studies in the literature have also been designed with reconfigurable components. Gong et al. designed a reconfigurable sensor testbed for autonomous vehicles [13]. This project aimed to create a design for a vehicle that is safe from control failure, among other common failures. Another example of testbeds designs with reconfigurable components in the literature is DRIVE, a communication system reconfigurable testbed designed in Madrid by Pinart et al. [14]. The reconfigurability of this testbed, simulating many radio and communication connections, will allow for the integration of many tests one would typically need multiple testbeds to emulate and determine the best communication system for the application.

Kaisheng et al. designed a single-shaft parallel hybrid electric vehicle powertrain testbed, focusing on developing hybrid electric vehicle control systems [15]. Regarding flexibility, Batteh et al. designed a virtual modular hybrid electric aircraft demonstrator system based on a NASA X-57 aircraft. The design for this architecture was created in Modelica and can simulate three electric aircraft configurations. This was the first step in a larger project to create a virtual and physical model [16]. Silva et al. created a Modelica model of a locomotive powertrain, resulting in component blocks that can be represent powertrains for other vehicles as well [17].

Simulation of Testbeds

After the conceptual base design of the vehicle is determined, simulations are run to analyze the system. A commonly used platform for simulating testbeds is MATLAB/Simulink, which will be used in this thesis. A range of organizations have used this method of testbed modeling, including many universities [18], [19], [17], [20] and NASA[1], [9]. A model of a system or multiple systems allows the user to identify components requirements, capture key interactions between components, and evaluate the performance of candidate systems quickly and inexpensively prior to experimental implementation [21]. The model of a hybrid aircraft testbed created by Knauff et al. aimed to experiment with different propulsion configurations and determine the best operating conditions. The testbed was modeled in Simulink and designed from the SimPowerSystems block set. However, the simulation was not reconfigurable, so each configuration was made separately, and the results of each were compared [18].

Williams created an aircraft power system model in Simlink. The powertrain was simulated to test how well a new control algorithm performed as compared to a basic proportional-integral controller [19]. The control systems were rated on fuel consumption and thermal regulation performance. At the University of Louisiana State University, Dehesa et al. created a hybrid electric powertrain model in Simulink that tested control strategies [20].

Roberts took a slightly different approach to determine the best control strategy for an aircraft [22]This research aimed to model an energy management system in Simulink that could eventually integrate with many different simulated propulsion and electrical systems for aircraft optimization. Systems were simulated individually to test the interface with the designed energy management system, since the simulation was not able to reconfigure between different propulsion and electrical configurations.

NASA's Information and Electronics System Laboratory at the Marshall Space Flight Center and the NASA Glenn Research Center have simulated testbeds for many different uses, including electrical power systems of large spacecraft and hybrid electric transport air vehicle powertrains [1], [9]. The creation of autonomous large power system breadboards by NASA led to the implementation of a computer-based simulation to evaluate the combination of these power system breadboards that allow the testing of any power system idea. These boards are currently planned to inform missions to Mars, the Moon, and the International Space Station [9]. The NASA Electric Aircraft Testbed (NEAT) emulates a single-aisle transport air vehicle with a hybrid electric powertrain. Simulation of this testbed was used to produce test data that could be compared to the results of the physical testbed created earlier. This testing ensured that the simulation ran correctly when scaled up or down [23]. The main challenge of this physical testbed was that it was difficult to reconfigure for the electronics to handle increased inputs or higher power.

Limiting the need for multiple testbeds or rearranging testbeds is the driving goal in the research of this thesis. The key difference between the above sources and the work done in this thesis is that none of the designs mentioned can simulate reconfigurable powertrains. Reconfigurable sensors and communication systems help test small parts of the aircraft. A reconfigurable powertrain testbed will allow the simulation and testing of completely different aircraft setups.

Implementation of Physical Testbeds

The last step in creating a physical testbed is to instrument and integrate the hardware components represented in the simulation. Some companies and agencies that have developed full-

scale testbeds for hybrid electric powertrains include GE, Collins Aerospace, Rolls-Royce, Airbus, and NASA [24]. The NASA Glenn Research Center in Cleveland, Ohio, developed a plan for ground testing of a hybrid electric MC-12 aircraft [24]. The motivation for this work is derived from the different roles that turbines play in electric aircraft powertrains versus fuel-powered aircraft powertrains. There has been little development in testing how these turbines will act in electric aircraft in different flight conditions. NASA developed a simulated altitude testing program that can couple with their full-scale hybrid electric powertrain testbed to test how the electronics perform in these different conditions.

Crow et al. created Triton: a reconfigurable software testbed for avionics [8]. This software can be interfaced with physical components to test scenarios with components that cannot easily be tested in a lab due to size or other limiting constraints, like a large engine. Since all the wiring connections of components are simulated through the software, the testbed is easily reconfigurable and does not include the need to unplug components. Some works focuses on reconfigurability by making the testbeds portable for use in multiple facilities. Srivastava et al. designed a control system testbed for US Navy ships with the main goals of portability and flexibility [25]. Flexibility was defined as the testbed being able to test different control configurations. The literature explains that flexibility will be achieved by simulating different components to that can be adapted to represent different control structures while keeping the physical components in the same place.

On the ground, Rangesh et al. developed a car-like vehicle testbed to support the development of autonomous driving [26]. This testbed includes many sensors and cameras that allow for collecting a large amount of data to be analyzed to improve the decision-making and planning of autonomous driving systems.

Yang, Guo, and Ye developed a hardware-in-the-loop simulation that incorporates physical components like dual motors and control components with a Simulink model that can be run in real time [27]. Tests run on the system include looking for weaknesses in avionics that can be exploited by cyber-attacks. An example of a software reconfigurable testbed comes from Thanagasundram et al., who created a reconfigurable hardware-in-the-loop simulator [28]. This simulator is connected to electronic controller units in a ground vehicle. Because of the flexibility of the software, once the simulator is connected to the controllers, the connections do not need to be changed. Instead, if rewiring was required, the software changes the signal routing to match the correct pins and interfaced with sensors and actuators.

The University of Illinois has created several small-scale testbeds to evaluate propulsion configurations and control algorithms [29], [30], [31]. Creating physical testbeds, even on a small scale, can help assess design parameters and test candidate control algorithms. Pieper, Perry, and Ansell created a small-scale Cirrus SR22T and tested the aircraft powertrain in a wind tunnel [29]. The wind tunnel results were then used to develop ground testbeds to evaluate the powertrain further. The most significant limiting factor found throughout these tests was the limitations of battery capacities. Aksland and Alleyne used a small-scale testbed to validate control algorithms. The testbed for these control configurations represented a series hybrid UAV powertrain [31].

Airborne Testbeds

Though most testbeds are stationary on the ground, there are a few examples of flying testbeds. Often, these testbeds are scaled-down versions of the final product to test the desired system's safety, functionality, and integration before being placed in a production vehicle. This

approach can save money and result in fewer large-scale failures of the developed aircraft. Pfeifle et al. developed both a manned and unmanned flying testbed to evaluate different control algorithms for distributed propulsion electric aircraft [32]. The testbeds were similar in configurations but differed in which components were used for yaw control, alternating between the propellers mounted on the wing tips and using differential thrust and manual control surfaces.

A larger-scale airborne testbed is NASA's Subsonic Research Aircraft Testbed (SCRAT) [33]. SCRAT can execute in-flight experiments that can test many components like sensors, instrumentation, and new systems. NASA Langley Research center has other testbeds capable of flying, like the Airborne Subscale Transport Aircraft Research (AirSTAR) testbed [34]. This testbed focuses on verifying the safety of new control systems. The testbed is small in scale and can be flown remotely. The control system is on a testbed on the ground, allowing easy access for changes during experimentation. This testbed aims to create control systems that can restore control when a system fails in flight. NASA has also developed a turboelectric distributed propulsion testbed aircraft based on a TG-14A motor glider. This flying testbed can experiment with different technologies aboard the aircraft [35].

Pieper designed a distributed electric propulsion testbed aircraft that can be implemented in a Cirrus SR22-T airframe [36]. Pieper created a small-scale radio-controlled model that consisted of the testbed inside the airframe. A test stand was also developed to experiment with the wing configurations' safety and determine that the powertrain chosen would be most beneficial for the desired experimentation. The small-scale model underwent experimentation in flight tests rather than a wind tunnel to obtain as accurate data on the vehicle performance as possible.

Again, basing the airframe on previously created aircraft, Joels et al. created a 3D-printed small-scale replica of the Lockheed Martin Body Freedom Flutter called the Active Aeroelastic

Aircraft Testbed (A3TB) [37]. This model was fitted with an electric engine and propeller and placed in a wind tunnel to evaluate different propeller performances and propulsion system configurations, verifying that the selected configuration was ample for flight testing. The A3TB was tested mostly on the ground but had one maiden flight test.

The UK Empire Test Pilot School's Bagel Basset Aircraft operates with a reconfigurable control system [38]. This allows the aircraft's control surfaces to be manipulated in different ways that result in varying flying quality of the aircraft. Because of this adaptation, different control algorithms can be analyzed so the aircraft can fly in the optimized mode based on different missions.

Many of these testbeds, even though they are airborne, follow the same design and simulation processes as ground testbeds. Each flying testbed first verifies that the propulsion configuration chosen works through wind tunnel testing or other ground testing. A reconfigurable powertrain testbed would increase the possible aircraft options and performance capabilities. Building on the literature above, this thesis describes the simulation and design of a small-scale hybrid electric aircraft testbed.

Chapter 3

Dynamic Model of the Propulsion Configuration

Component Block Models

A dynamic simulation model was created in Simulink to aid in designing the testbed. Electro-mechanical components like motors, inverters, electrical buses, and more were modeled as blocks that capture the governing equations, following the derivations in [30]. Examples of blocks in the toolbox are shown in Figure 4. An example of the subsystem inside the motor block is shown in Figure 5. Within the subsystem, the governing equations of the system are coded as MATLAB functions. For example, the code to calculate the angular speed output of the motor is within the "Omega" block in the top right corner of Figure 5.

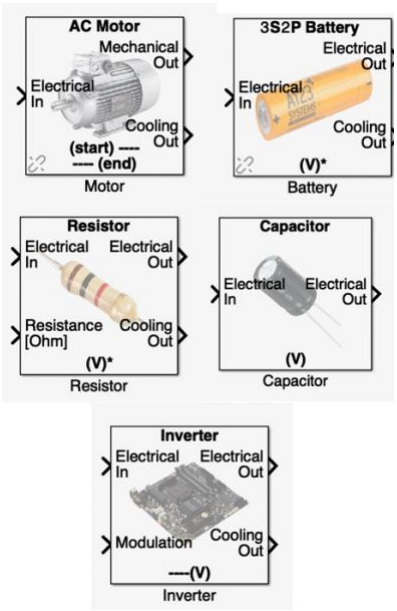

Figure 4: Examples of Blocks in Modeling Toolbox

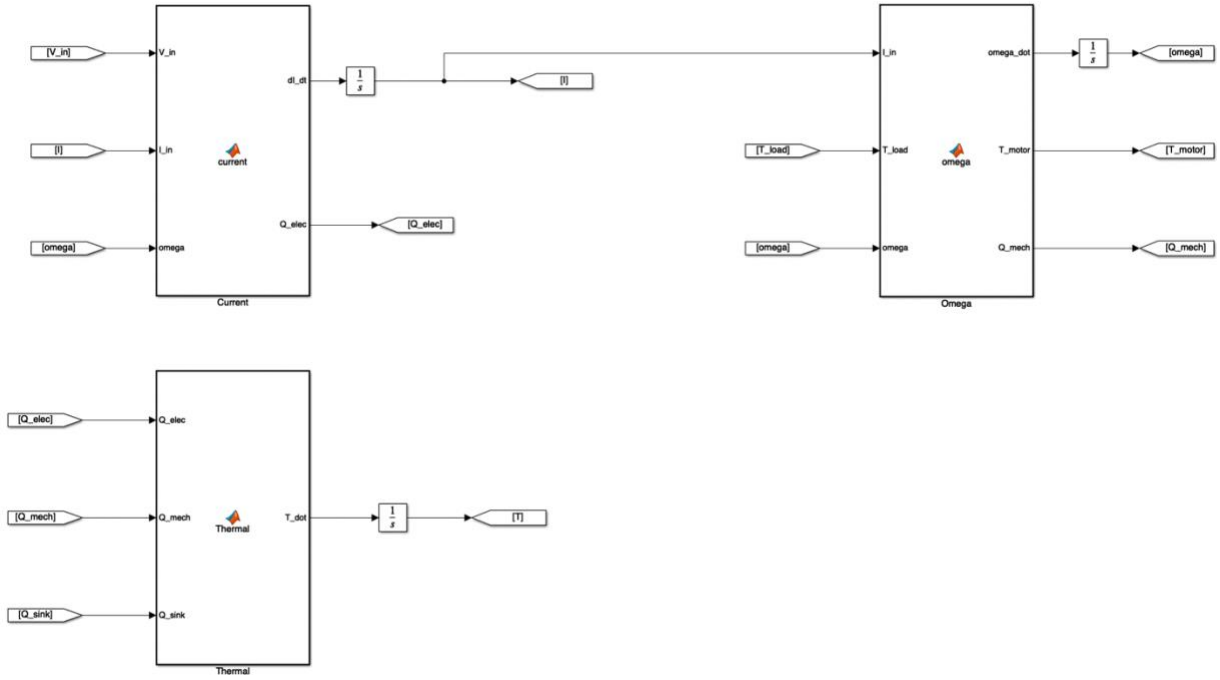

Figure 5: Inside the Motor Block from Modeling Toolbox

A block diagram was created to visualize the signals sent between component blocks when assembled into a powertrain model, as shown in Figure 6. A voltage source, inverter, motor, generator, and load were needed to simulate a basic electric power train. Each electro-mechanical component was also connected to a thermal management system consisting of a heat sink and temperature sink. The block diagram shows the direction in which voltage, current and thermal signals flow between each block. For example, the motor takes an input of voltage, angular speed, and torque. The voltage comes from the previous “Y to Delta” converter block, which converts a block with wye wiring to a block with delta wiring. The different wiring types are shown in Figure 7. The inverter component is a wye wound device, while the motor is a delta wound device. The motor block calculates an angular acceleration. This value is then integrated and fed back as the

angular speed input to the motor block. The torque input to the motor comes from the generator block's torque output, which is fed back to the motor.

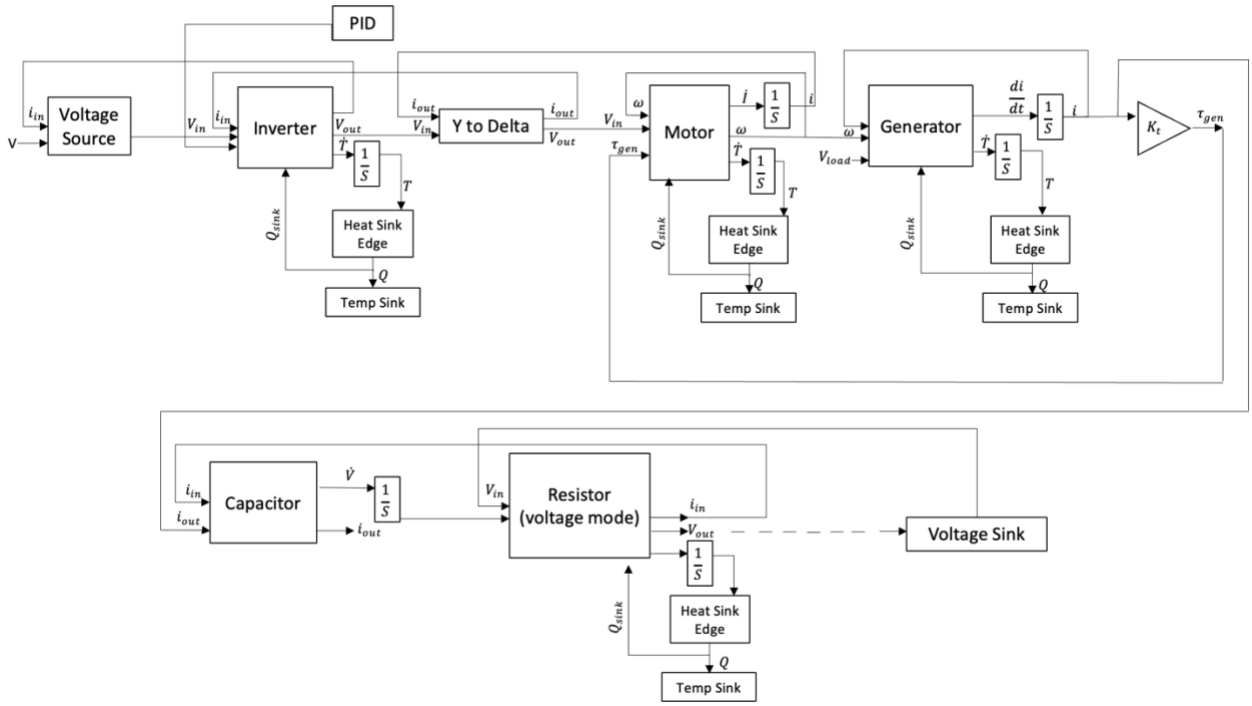

Figure 6: Block Diagram of Simulink Model

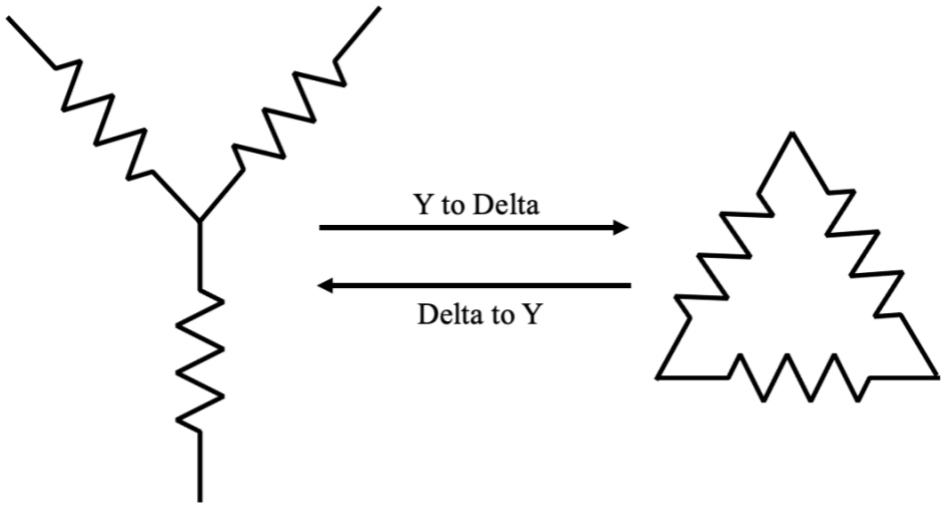

Figure 7: Y to Delta Conversion

Final Simulink Model

The final model of the electric powertrain configuration has eight different types of blocks. These blocks include a battery, bus, motor, inverter, generator, PID control, thermal sink, and constant boundary conditions for parameters such as speed reference. Smaller simulations were created, tested, and combined to implement these blocks. First, the motor block was tested. This model is shown in Figure 8 and includes a voltage source, motor, torque sink, and temperature sinks. Feeding the torque sink is a torque profile for a fixed-wing aircraft, provided by Dalton Decerio and Prof. David Hall of the Penn State Department of Aerospace Engineering [39] and shown in Figure 9. The large spike at the beginning of the profile represents the aircraft during takeoff. The torque profile slowly levels out as the aircraft transitions from takeoff and climb to cruise at a constant altitude. The decrease in torque after this steady period is the descent and landing. This torque profile was scaled to be appropriate for the motor sizing used in this simulation study. The 20kW motor torque data was scaled down by a factor of 1000 and could be scaled down further. A conversion factor of 1.35 was used to change the output data from ft*lb to N*m, as all Simulink blocks in the model assume metric units.

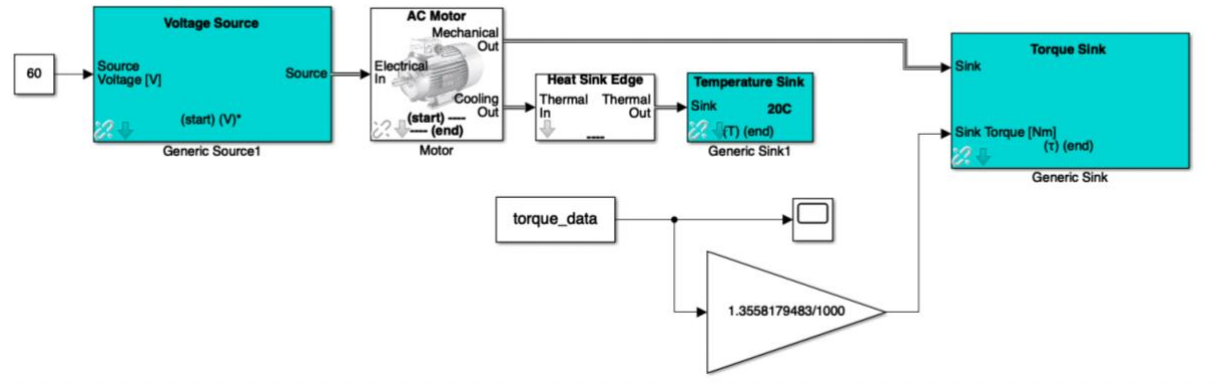

Figure 8: Simulink Model for Motor Testing

The torque profile and motor model were used to test different motor parameters. Specifically, changing the parameters and observing how this affected the simulated outputs helped to guide the choice of specifications for the physical motor to purchase for the experimental testbed. The design parameters for the motor are the armature resistance, motor constant, static friction coefficient, viscous friction coefficient, armature inductance, shaft inertia, initial total current, and initial speed.

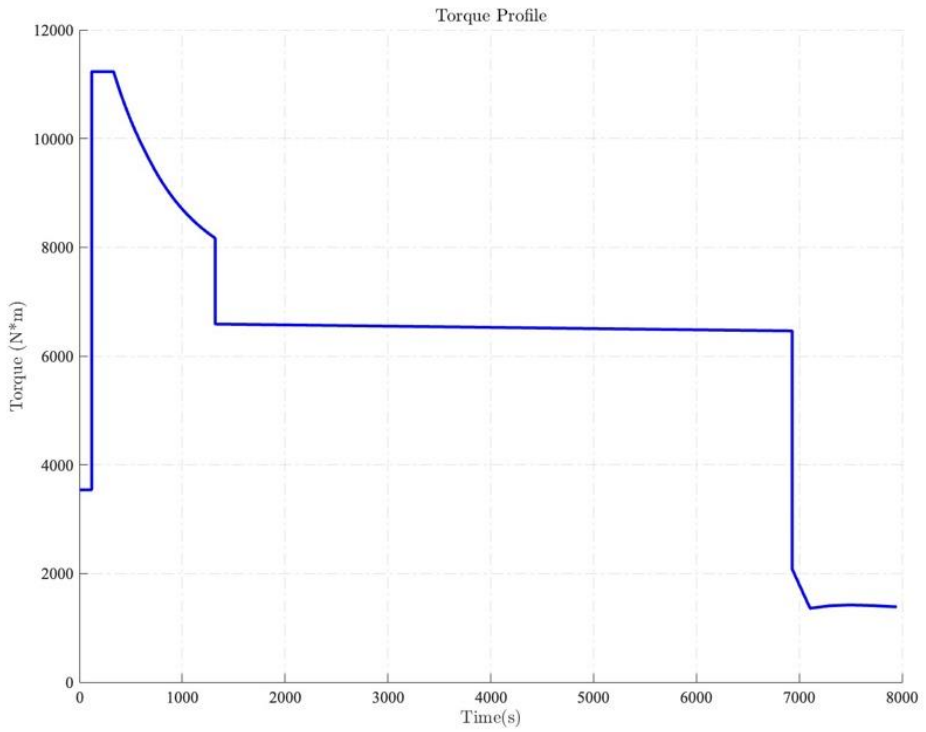

Figure 9: Fixed Wing Aircraft Torque Profile

Next, additional blocks were connected to the motor block to build a complete propulsion configuration. An inverter and a “Y to Delta” conversion block were added between the motor and the constant voltage source. A PID controller was also implemented in the model to regulate the

motor speed to around 1000 RPM. The updated model and motor state subject to the torque profile are shown in Figure 10 and Figure 11, respectively.

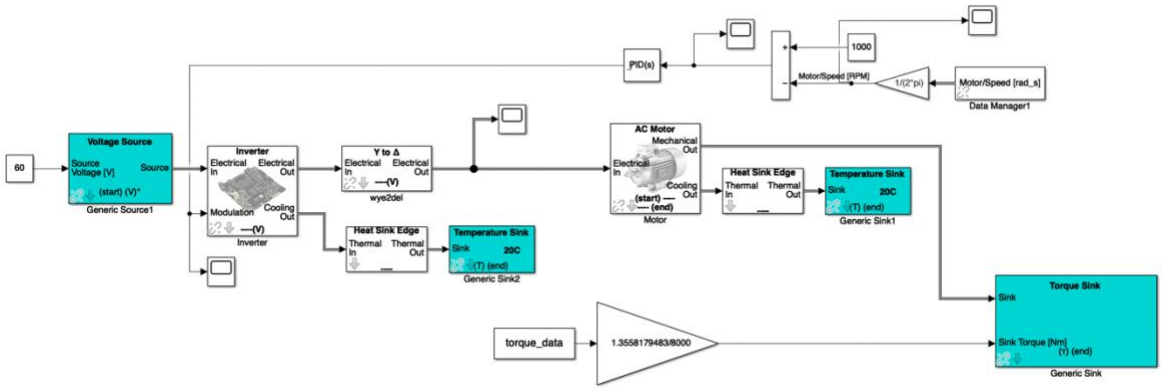

Figure 10: Simulink Model with Motor and Inverter

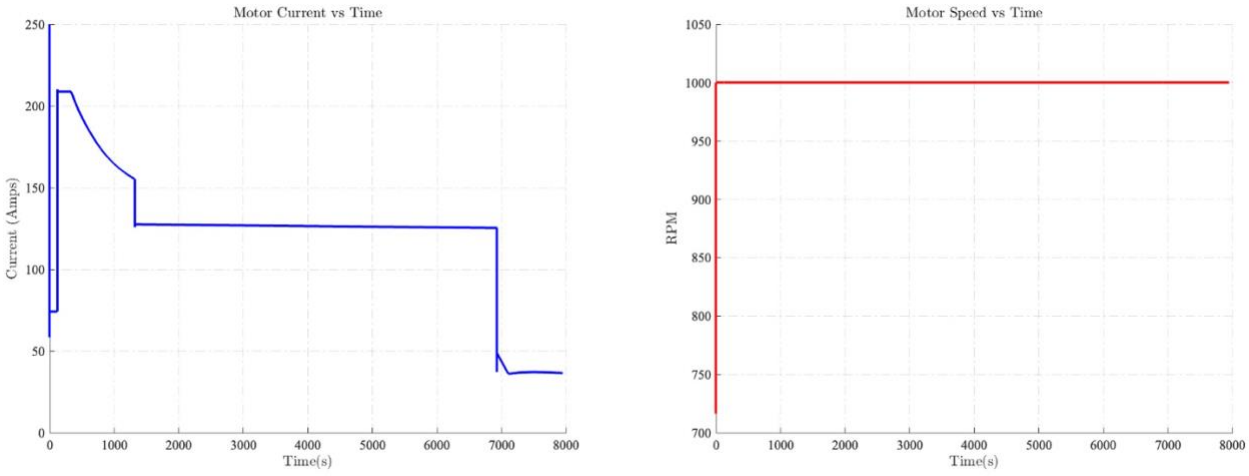

Figure 11: Motor Current and Speed vs. Time

The next step was to create a generator block, which had not previously been included in the component toolbox. The governing equations of the motor provided a starting point for creating this new block because the governing physics are the same, except that a motor converts an

electrical power input into a mechanical power output. In contrast, a generator converts a mechanical power input into an electrical output. The motor and generator governing equations are shown in equations 1-3 and 4-5, respectively [30]. The generator model takes the angular speed output of the motor and the load voltage as inputs and calculates the current derivative, which is then integrated to calculate the generator's current state. The current state is multiplied by a torque constant to calculate the generator torque.

$$\frac{di}{dt} = \left(\frac{1}{L}\right)(V_{in} - R * i_{in} - K_v * \omega) \quad (1)$$

$$\tau_{motor} = K_v * i_{in} \quad (2)$$

$$\frac{d\omega}{dt} = \left(\frac{1}{J}\right)\left[\tau_{motor} - \tau_{load} - b * \omega - c\left(\frac{2}{1+e^{-5\omega}}\right) - 1\right] \quad (3)$$

$$i = \left(\frac{1}{L}\right)(-V_{out} + K_v * \omega - R * I) \quad (4)$$

$$\tau_{generator} = K_v * I \quad (5)$$

In these equations, V_{in} is the voltage input to the motor, R is the resistance of the motor, i_{in} is the current into the motor, K_v is the torque constant, ω is the angular speed state of the motor, J is the shaft inertia, b and c are static and viscous friction coefficients, respectively, V_{out} is the load voltage, L is the inductance, and I is the integrated current from the generator. τ_{motor}, τ_{load}, and $\tau_{generator}$ are the torques from the motor, load, and generator, respectively.

After the generator block was created, its functionality was tested. To do so, a voltage sink and temperature sink were coupled to the generator, and this assembly was simulated. After it was confirmed that the generator block functioned as intended, it was connected to the larger powertrain model shown in Figure 12. The motor shaft was coupled to the mechanical input of the

generator, and a capacitor and resistor in series were coupled to the generator's electrical output to act as a load.

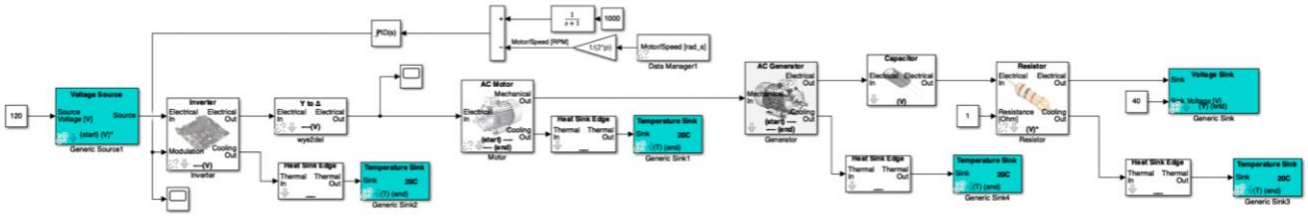

Figure 12: Adding the Generator

The resulting Simulink model was then simulated for 10 seconds, with a constant load and a PID controller for the inverter set to track a motor speed reference of 1000 RPM from an initial speed of 0 RPM. Figure 13 shows that the controller can achieve and track this reference.

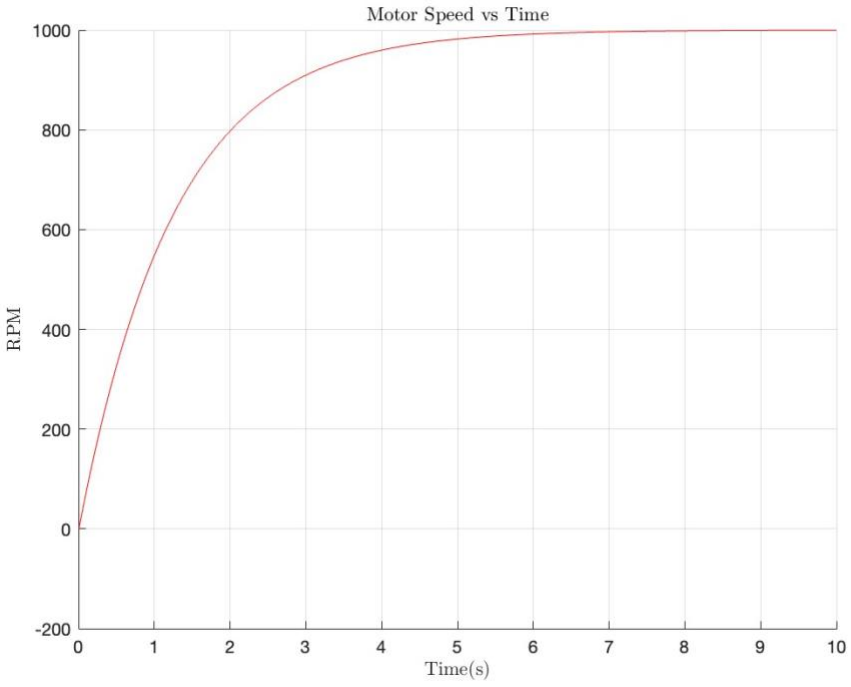

Figure 13: Motor Speed vs. Time of Model with Generator and PID Control

Once the generator and motor were successfully coupled in the Simulink model, an electrical bus was added to allow two independent power sources to connect to the model of the propulsion configuration, forming a hybrid powertrain. The two separate power sources are a battery and a generator driven by an engine. In the Simulink model, a turboprop engine is modeled as a constant angular source to the generator. Trade studies can then be performed to study the power split between the engine and battery in supplying a constant load. The battery is modeled as an equivalent circuit with one cell for simplicity.

Adding the Torque Profile to the Final Model

The bus combines the power supplied by the engine and battery to drive the load. For a hybrid electric aircraft, the power split between the engine and battery can vary between different stages of flight. For example, during takeoff, the battery may be discharged at its maximum rate to reduce the peak power demand of the engine. Then during cruise, the engine may be used to both provide propulsive power and recharge the battery. The torque profile provided for a fixed-wing electric aircraft from Figure 9 was again scaled and applied to the motor to evaluate the hybrid powertrain simulation. The revised model with the torque profile added is shown in Figure 14.

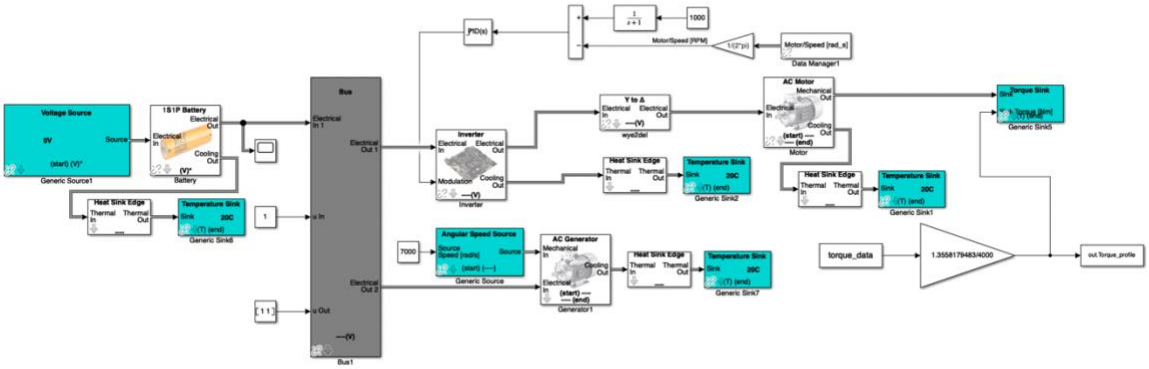

Figure 14: Series Hybrid Electric Model in Simulink

Figure 15 shows the battery's state of charge during the 130-minute simulation. This figure follows the expected pattern for a battery used in a hybrid electric aircraft. The battery initially decreases in charge as it provides supplemental power to the engine for takeoff. At the start of cruise, around 1300 seconds or 22 minutes, the battery is recharged slightly and then reaches a constant state-of-charge as the engine supplies all the power for propulsion. After about 7000 seconds or 120 minutes, the battery state-of-charge increases as the propulsive power demanded decreases during descent and landing, and additional power from the engine is stored in the battery.

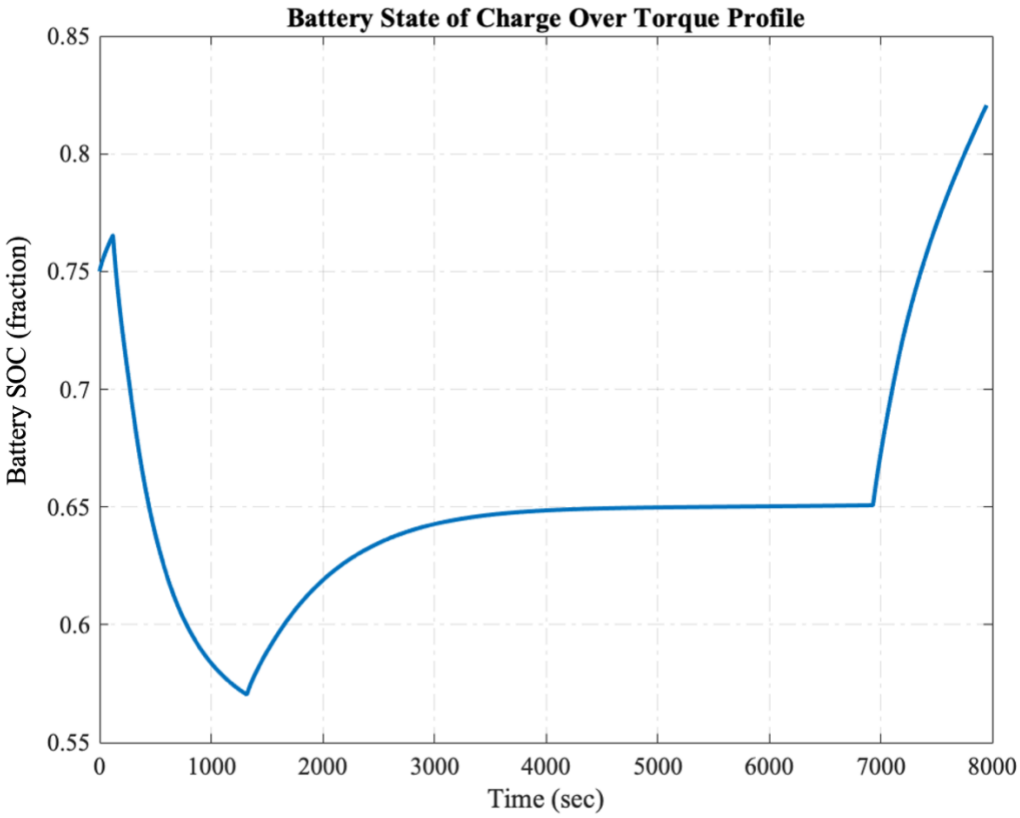

Figure 15: Battery State of Charge vs. Time for Given Torque Profile

With the powertrain simulation complete, results from these simulation studies were used to inform the desired sizing of physical components to purchase for the experimental testbed. Specifically, the model was used to determine target parameters for the motor, battery, and possible loads of the testbed. The parameters of the motor model used in the final Simulink model are shown in Table 1. These parameters were based on those in [30], shown in Table 2 which served as a starting point for the simulation and were altered to fit the torque profile.

Table 1. Simulated Motor Parameters

Motor Parameter	Value
Resistance (ohm)	0.01346
Motor Constant (Nm/A)	0.00969
Static Friction Coefficient	0.00023
Viscous Friction Coefficient (N*m*s/rad)	1.89435e-05
Inductance (H)	1.25219e-05
Shaft Inertia (kg*m^2)	1.09e-4

Table 2: Motor Parameters Used as Reference

Motor Parameter	Value
Motor Constant (Nm/A)	0.1238
Static Friction Coefficient	0.228
Viscous Friction Coefficient (N*m*s/rad)	0.360-03
Inductance (H)	4.87e-05
Shaft Inertia (kg/m^2)	2.73e-3

Chapter 4

Creating a Physical Testbed

To create a physical testbed, parts had to be selected for the desired end functionality of the system. The goal of the testbed is to eventually emulate many different propulsion configurations of a hybrid electric aircraft by becoming easily reconfigurable without the need for moving or disconnecting parts already on the testbed.

Selecting Parts

First, motors were ordered, as two were used and coupled in the testbed. The motors selected for this testbed were model 6515 from Neu Motors. The specifications and sizing for these motors are shown in Table 3 and the datasheet can be found in Appendix A. These motors are rated to a maximum speed of 12000 RPM, which exceeded that expected to be needed for experimentation with the testbed. The speed capability and the small size of the motors motivated their selection. The motor is shown in Figure 16.

Table 3: Neu Motor 6515 Parameters

Motor Parameter	Value
Resistance (ohm)	0.115
Torque Constant (Nm/A)	.018910
Shaft Size (mm)	8
Diameter (mm)	76

Length (mm)	47
Max Volts (V)	24
Max Amps (A)	211
Max RPM	12000

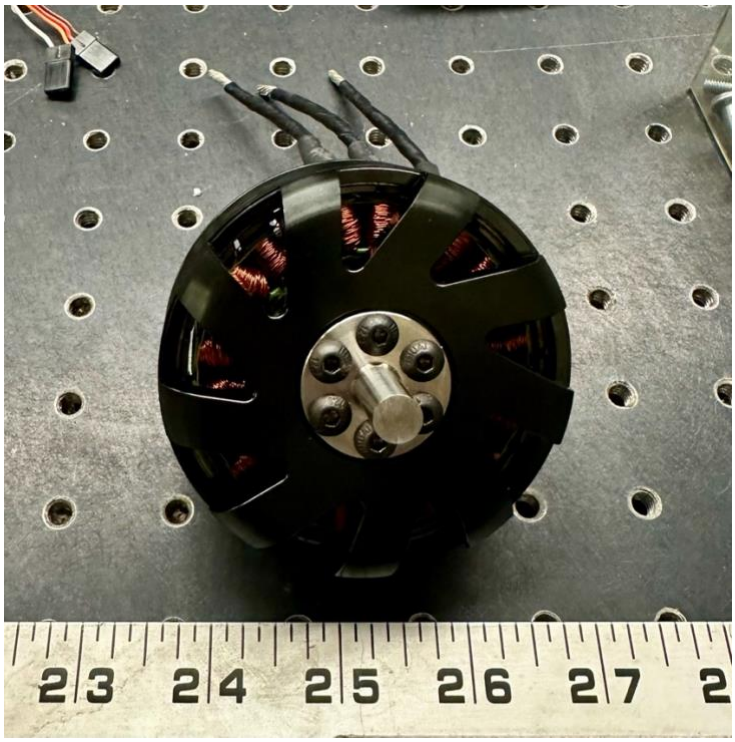

Figure 16: Neu Motor 6515

More components were ordered for the testbed using information from the Simulink model of a hybrid electric powertrain. A Phoenix Edge HV speed controller from Castle Creations was ordered to control the motors. A shaft coupling was also ordered. The goal of the shaft coupling was to prevent misalignment and vibrations. The shaft coupling selected was a MIC-5-0617 Coupling from Magtrol with a rated torque of 6.17 Nm. The calculated torque required for the

shaft coupling was 3 Nm. A Magtrol TS 106 torque transducer was selected to read the speed and torque measurements from the motors. The specifications for the parts in the testbed are in Appendix A.

Design of Mounts

Once the motors were ordered, they needed to be safely mounted to the testbed. Multiple motor mount designs were considered, and the advantages and disadvantages of each were analyzed. The goal was to have an easily adjustable motor mount that ensured correct alignment of the two motors. The first design is shown in Figure 17. The design consists of an aluminum angle and a piece of aluminum 80/20 slotted extrusion. A single 80/20 beam would be used to mount two motors together, and another aluminum angle for each motor would be screwed into the 80/20. This configuration allows for adjustment of the distance between the motors and precise alignment of their shafts since the aluminum angles will be connected to the same piece of metal.

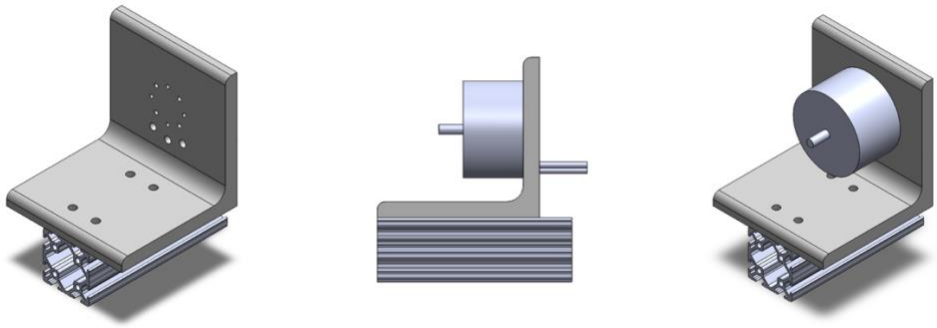

Figure 17: First Motor Mount Design

The motor can be mounted on the aluminum angle's front or back side. Motors mounted on the front side result in less force on the bottom aluminum angle screwed into the 80/20 since

the center of gravity is above where the plate would be secured. However, since the motor is above the screws, it is harder to adjust the horizontal placement of the mount once the motor is mounted in this configuration. The motor could also be mounted opposite the way shown in Figure 17, allowing easier access to the screws attaching the mount to the 80/20.

There are some disadvantages of this design to consider as well. An aluminum angle would be hard to machine with a CNC or water jet cutter and would likely have to be machined by hand instead, which may result in lower precision and, therefore, worse alignment of the motors. The primary disadvantage to this design is that the height of the motor mount is fixed. To raise the motor's height, one would have to increase the height of this motor mount by placing something underneath it. In other words, the motor mount does not have an easily adjustable height.

An adjustable height was determined as a critical characteristic of the motor mount because the entire testbed had not been fixed. The necessary height for the motor was undetermined, so a flexible motor mount was required. A second motor mount was designed to incorporate this characteristic. The idea for this motor mount is shown in Figure 18. This design consists of four pieces of 80/20 aluminum and one flat aluminum sheet.

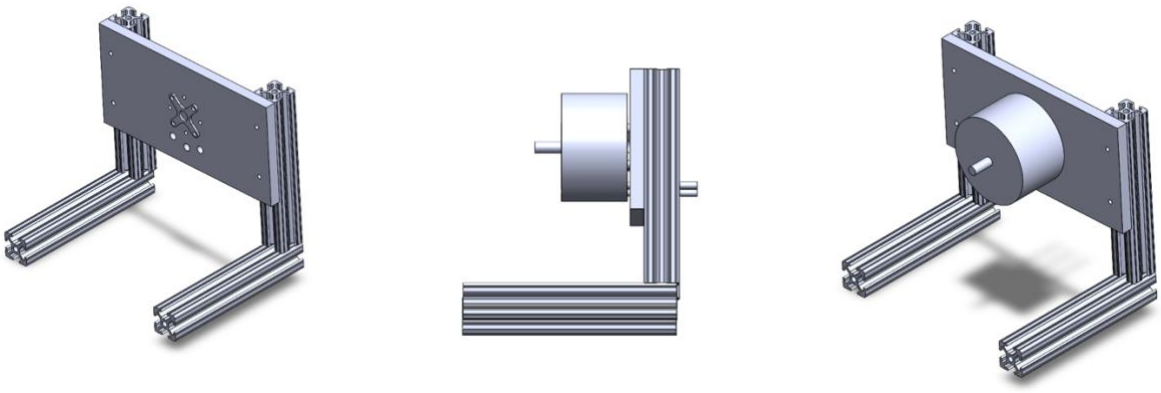

Figure 18: Second Motor Mount Design

There are two main advantages to this design which are as follows: the height is easily adjustable by screwing the aluminum sheet in at different heights, and the flat aluminum plate is easily machinable with a CNC mill or a waterjet. Since the aluminum plates can be easily machined, they are more likely to be close to identical in terms of hole placement, resulting in more accurate alignment. The horizontal distance between motors can also be adjusted in this design as the two vertical 80/20 pieces can slide along the horizontal 80/20 pieces. A disadvantage of this mount having adjustable height is that both motors must be adjusted to the same height to ensure correct vertical alignment.

Considering the advantages and disadvantages of each design and the critical design characteristics needed for the motor mount, the second motor mount design was chosen to prototype. Regarding the disadvantage of alignment with adjustable height, identical stoppers would ensure that each plate is as close to the correct height as possible.

Prototype of Mounts

After the second design was selected, a 3D-printed model was created from an updated version of the CAD file. This model was made from PLA filament. The 3D-printed motor mount was attached to two pieces of 80/20, as shown in Figure 19. The updated motor mount has only four holes in the center to connect to the motor, as this number was determined sufficient to hold the motor in place. Instead of three holes toward the bottom of the mount for the connecting wires, one larger hole was formed for quicker assembly and easier cable access. The 80/20 pieces were held together with right-angle connectors and screws and temporarily mounted to the table with clamps.

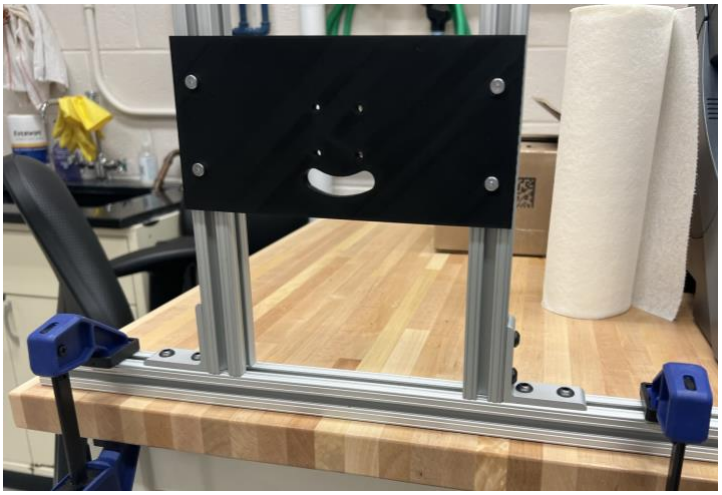

Figure 19: First Motor Mount Prototype

Assembly of Mounts

After screwing the motor into the prototype mount, it was noticed that the motor was not flush against the mount. This was because there is a small part on the back center of the motor that sticks out farther than the rest. To compensate, a large hole was drilled in the center of the mount so the motor could lay flat. These adjustments are shown in the right photo of Figure 20. The left image of Figure 20 shows the mount and motor fixed in place after the adjustments described were completed.

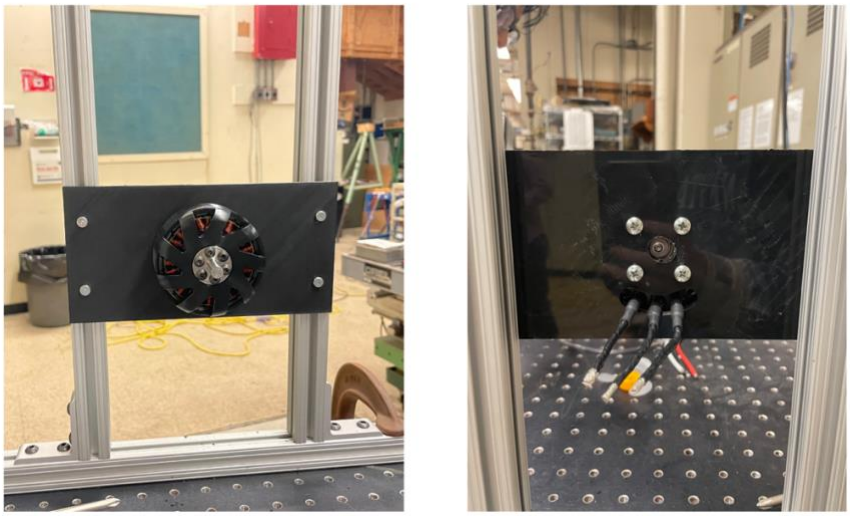

Figure 20: Adjusted Motor Mount Prototype

The adjusted dimensions and extra hole in the center were added to the CAD model of the motor mount. This file was then sent to Origin Labs, a maker space at Penn State University, to have the mounts machined out of quarter-inch aluminum sheets. The aluminum machined motor mounts from Origin Labs are shown in Figure 21.

Figure 21: Aluminum Motor Mounts

The final assembly with an aluminum mount is shown in Figure 22. Before the two motors could be mounted and run together, it had to be proven that one motor could run and be controlled safely, which will be discussed in Chapter 5.

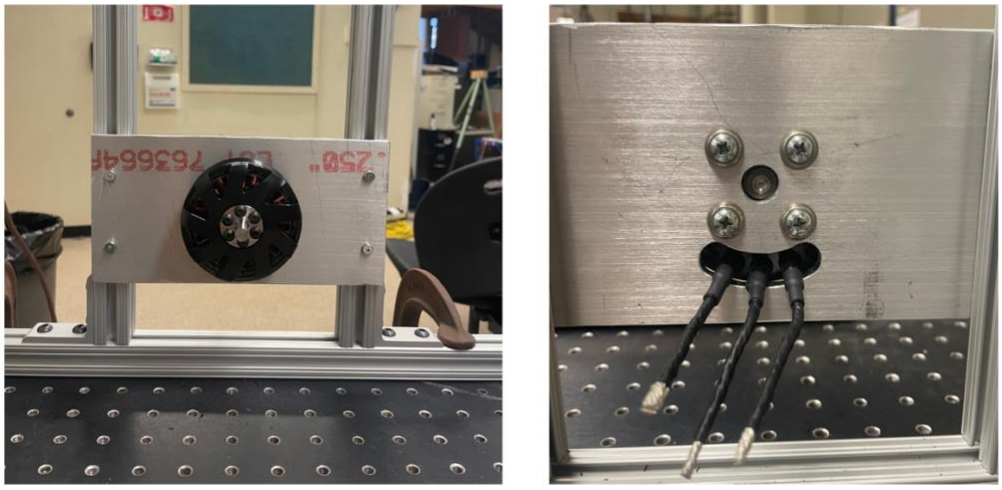

Figure 22: Motor on Aluminum Motor Mount

Design of Testbed

After the design of the motor mounts was validated, the entire testbed design was considered. First, the area allocated for the testbed was determined. Due to the space available in the lab, a two-foot by three-foot testbed cage was designed, considering the layout could be scaled larger if needed. After the initial size was outlined, the next step was determining how many motor mounts would fit into the testbed. Due to the size of the testbed and motor mounts, two or three motor mount pairs can fit in the allotted space in different orientations. The spacing of motor mounts in different testbed designs is shown in Figure 23.

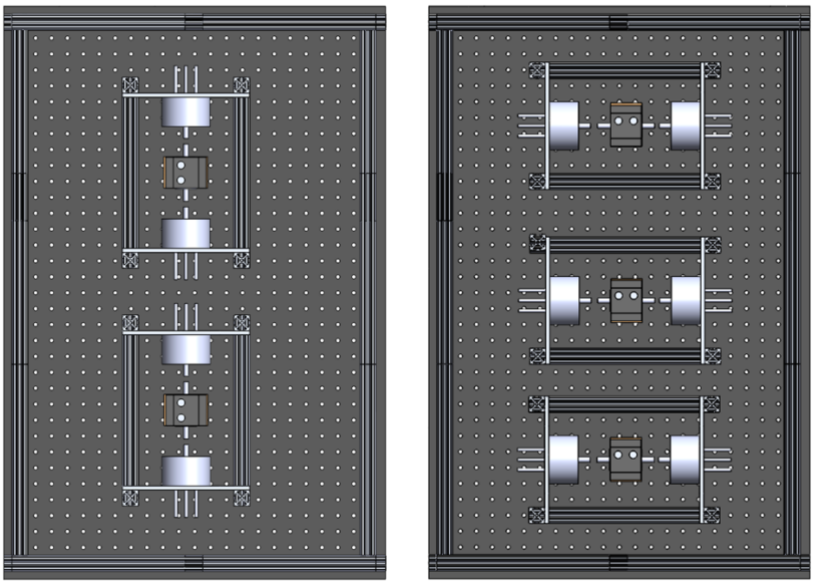

Figure 23: Motor Mount Pair Layout Options (Top View)

The advantage of the layout on the left of Figure 23 is that each motor mount pair has a different axis of rotation. Due to the momentum of the motors when they are spinning, a catastrophic failure would result in parts being ejected perpendicular to the direction of rotation. In the case of the layout on the left, the axis of rotation is along the front and back of the testbed so that parts would be ejected to the right or left. Therefore, one motor mount pair failing would be less likely to cause damage to other pairs in the testbed. For either layout, a cage will encircle the entire testbed to protect the rest of the lab and its occupants.

In the layout on the right of Figure 23, the axis of rotation is horizontal, and therefore parts that become loose would be ejected in the direction of the shorter end of the testbed. Since this is the smaller side of the testbed, it is easier to reinforce the sides of the cage to ensure that parts cannot break through, and it is easier to implement a no-stand zone where people working on the testbed must stand to the sides of the testbed, not to the front or the back. Three motor

mount pairs will fit in the testbed with the allotted area, and the layout on the right of Figure 23 was selected to continue development.

The testbed needs a cage for the safety of the people working around it. The material chosen was plexiglass since it can be easily cut to the desired sizes and shapes with a laser cutter and is available in different thicknesses. The inside of the testbed needed to be easily accessible, so a falcon wing door design was chosen for the first design. Having falcon wing doors, shown in Figure 24, allows for easy access to both sides of the testbed and, therefore, access to all the motor and speed controller connections. The doors would be mounted to an 80/20 beam with flat hinges. The material needed for this testbed design was calculated and shown in Table 4 and totals about 52 feet of 80/20.

Figure 24: Testbed Design Isometric View

Table 4: Testbed Material List

Material	Number of Pieces
35in 80/20	5
33in 80/20	2
12in 80/20	10
11in 80/20	4
9in 80/20	4
Brackets	30

Chapter 5

Testing the Testbed

The testbed was built in small pieces, ensuring each component worked adequately before attaching the next. Connecting the testbed in this way was ideal for troubleshooting. One could troubleshoot each component separately and join them once they ran successfully.

Testing the Motors

The first step was to run the motor unloaded. For the motor to run, it must be connected to the speed controller. The speed controller regulates the power sent to the motor. Full power correlates to full throttle of the motor, while zero power correlates to zero throttle. By controlling the amount of power sent to the motor, one can control the speed at which the motor runs. Three signals are sent to the electronic speed controller (ESC). These signals are a power input (+5V), ground, and a pulse width modulation (PWM) signal. These are the same types of signals seen in a servo motor. Because of these similar connections, the brushless motor can be treated like a servo and controlled similarly.

The PWM signal is a square wave with a varying duty cycle, describing the percentage of time that the signal is at its maximum or minimum voltage. For a servo motor, the standard signal is a 50 Hz PWM signal with a duty cycle between 1-2 milliseconds at maximum voltage. One millisecond results in minimum speed from the motor and two milliseconds in maximum speed. Before the motors were run, the output signal was tested to ensure it was the desired 50 Hz PWM.

Creating a PWM Signal

To create a 50 Hz PWM signal, an Arduino Mega 2560 was used. The Arduino can create many different PWM signals. By importing the servo library into the Arduino code, a 50 Hz signal was generated. The end goal of the Arduino code was to have the Arduino output a PWM signal whose duty cycle was controlled by a user specifying the desired percentage. This task was broken into parts. First, the duty cycle percentage was controlled by turning a potentiometer wired to the Arduino and displayed on an oscilloscope. Then the potentiometer was replaced by text inputs communicated to the Arduino using the serial monitor. Lastly, the PWM output from the Arduino was wired to the ESC and used to run the motor.

The potentiometer and servo pin must be identified in the Arduino code to create a PWM signal from the servo library. The servo pin was defined as pin 9, and the potentiometer pin was defined as A0. This definition means that the PWM signal to the ESC came from pin 9, a digital pin. The input from the potentiometer came from pin A0, which is an analog pin. When a potentiometer is turned to its minimum value, this is read by the Arduino as an ouput of 0. When a potentiometer is at its maximum value, this is read by the Arduino as an output of 1023. To achieve the desired PWM signal output, the command to the servo library function requires an argument between 1100-1900. Because of the difference in these ranges, the potentiometer values needed to be mapped to the servo range. This was done with a one-line command in the Arduino code. The mapped signal is then written to the output pin (pin 9). This relation allows the potentiometer values to be taken as inputs, converted to appropriate values for the servo library, and used to set the output PWM. The Arduino circuit shown in Figure 25 was created to run the code described above, as seen in Appendix B. The goal was to have the oscilloscope (the yellow box in Figure 25) output a PWM signal that would change as the potentiometer was rotated.

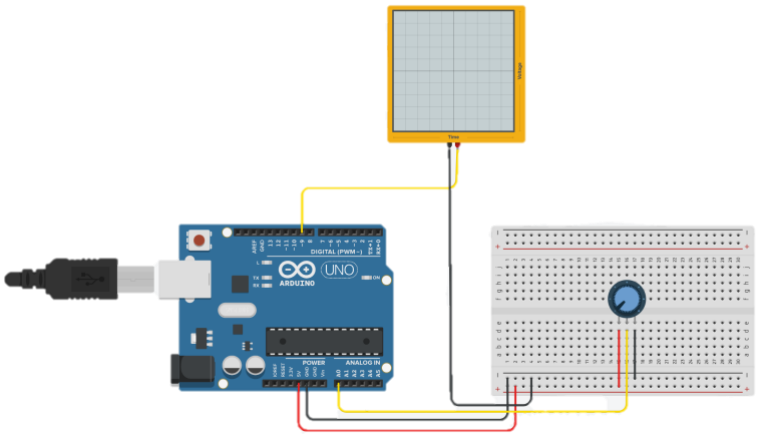

Figure 25: PWM Signal Testing Circuit

After the circuit and code successfully produced a PWM signal, the next step was controlling the PWM signal via the Arduino serial monitor instead of a potentiometer. The serial monitor is a connection between the Arduino and the computer that can send and receive information between the two interfaces. The serial monitor was programmed through Arduino to receive a string from the input field. This string was then converted to an integer. Using the mapping function again, the Arduino converts the integer to a servo value. The possible inputs into the serial monitor were set as 0-100. These numbers represent the speed percentage of the motor, with 100 being full speed and 0 being stopped. This conversion allows users to input the percentage of the maximum motor speed at which they would like the motor to run. The serial monitor is programmed to output the current speed percentage and the corresponding PWM value. Figure 26 shows the slight difference in the PWM signal that results in the motor's maximum to minimum speed change. The figure on the left side represents an input of 0%, while the right represents 100%.

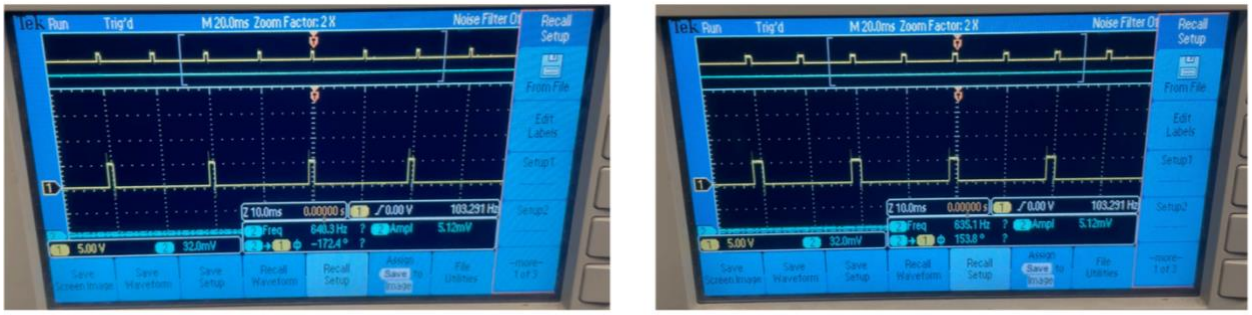

Figure 26: Range of PWM Signals Sent to Motor

Finally, the ESC and motor were connected to the Arduino circuit. Three output wires from the Arduino are attached to the ESC. The PWM signal comes from pin 9 and is attached to the orange signal wire on the ESC. The 5V and ground wires are connected to the ESC's red and black wires, respectively. The ESC has a three-phase output corresponding to power, ground, and input signals. These are attached to the three wires coming out of the motor using alligator clips for these experiments until a permanent connection to the motor can be determined.

Running the Speed Controller

The ESC only turns on when the minimum throttle signal is given. This safety feature ensures the motor does not automatically start at full throttle. When the speed controller is armed with the minimum signal, it plays a few beeps to let the user know the signal has been received and it is safe to increase the input. The minimum arming signal for the speed controller is not necessarily the same as the low value for a servo, which is sent from the Arduino. A servo ranges from 1100 to 1900, equivalent to 1.1-1.9 milliseconds. The arming signal of the ESC could range from 1.0 to around 1.3 milliseconds, so the exact minimum value needed to be determined by

experimentation. For preliminary experimentation with the motor and testbed setup, the chosen value for the arming signal was 1000, equivalent to one millisecond.

Simulating the Engine

A turboshaft engine model was created in Simulink by a former undergraduate in Dr. Hall's propulsion laboratory, James Bennick [40]. Bennick created an engine using multiple subsystem blocks in Simulink. The final turboshaft block could be integrated into the series hybrid electric model shown in Figure 14, replacing the angular speed source. The integrated model can be seen in Figure 27.

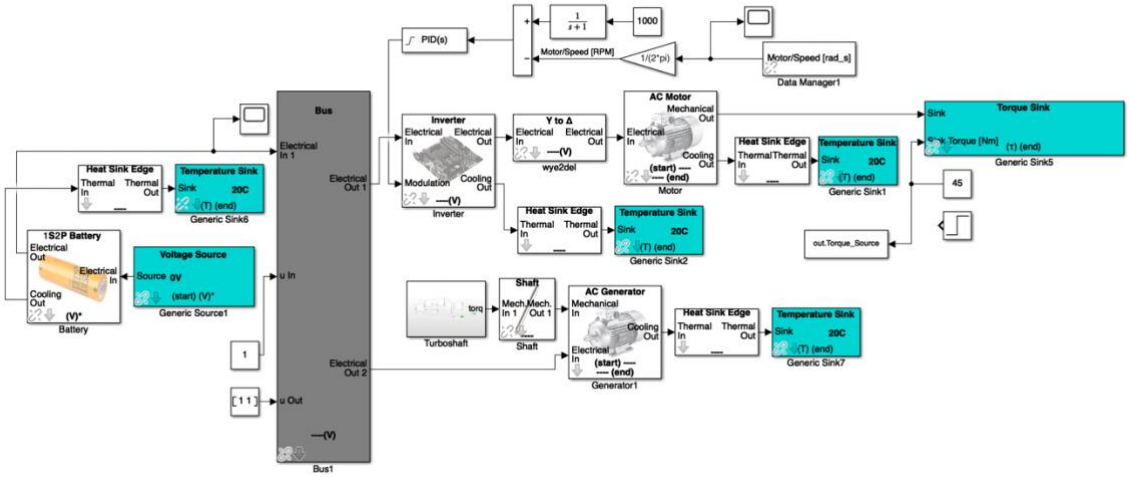

Figure 27: Hybrid Propulsion Configuration Model, Turbo shaft block from [40]

An Arduino can be connected to Simulink, run the calculations of the Simulink model, and send signals to the motor in the testbed. The MATLAB and the Simulink Arduino Support Package can be used to deploy the Simulink engine model to Arduino code. Using an Arduino to run the generated code, the Arduino could read the motors' outputs and calculate the response of the

modeled engine to those outputs. A feedback loop is then created to produce a desired shaft speed that can be sent back to the motor controller.

Connecting Simulink to Arduino

To couple the physical motors to a simulated engine, it is desirable to control the motors with Simulink. As discussed, the motors are connected to an ESC, which takes a PWM input. Initially, the code for the Arduino connected to the ESC was written in the Arduino IDE to create the PWM signal. By connecting the Arduino to Simulink, the output of the engine model, a speed command, can become the input for the desired speed. Therefore, the controller's speed can be regulated by changing engine inputs.

The Simulink Support Package for Arduino Hardware and MATLAB Support Package for Arduino Hardware were used to interface the Arduino and MATLAB/Simulink. Pin 9 was designated to be connected to the ESC. Therefore, an Arduino block in Simulink was used with pin 9 as the output. For this block, the desired frequency is specified as a parameter input in the range of 0-255 controls the duty cycle, where 0 corresponds to a duty cycle of 0%, and 255 corresponds to a duty cycle of 100%. The speed controller needs an input between one to two milliseconds. Therefore, this input to the Arduino block must be mapped so that the range one can specify for the PWM signal falls within the accepted limits. 1-2 milliseconds correspond to a 5-10% duty cycle, where 5% of 255 is 12.75, and 10% of 255 is 25.5. These limits were rounded to 12 and 26 to span the full range of the 5-10% duty cycle. The user input was selected as a sliding gain from zero to one representing the desired speed fraction. The input is then converted to a number between 12-26 to achieve the correct duty cycle range, and this final number is sent to the

Arduino output pin, which is connected to the speed controller. An example of the Simulink to Arduino conversion is shown in Figure 28. The constant value input on the left can be replaced by a speed output from the engine Simulink model, linking the engine and the motor.

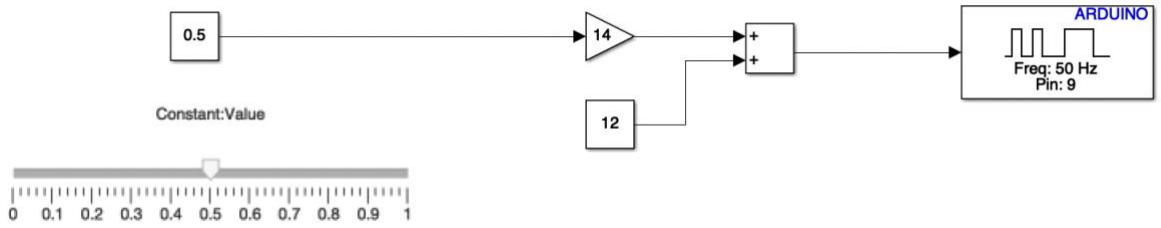

Figure 28: Simulink to Arduino Motor Control Setup

Connecting Simulink to the ESC

Once the Simulink to Arduino connection was tested, the simulation was connected to the hardware. Two motors were coupled using a Magtrol MIC-5-0617 coupling. The motor mount hardware was built following the designs discussed in Chapter 4, as shown in Figure 29. First, a computer with the Simulink model in Figure 28 was connected to an Arduino. Next, pin 9 of the Arduino was connected to the orange input signal of the ESC. The 5V and ground pins on the Arduino were connected to the red and black input signals of the ESC, respectively. A battery, supplying 20 V, was connected to the ESC as well. The three ESC output cables were connected to the three input cables of one of the motors. Finally, the second motor was connected to an oscilloscope so the output signal of the coupled motor could be evaluated.

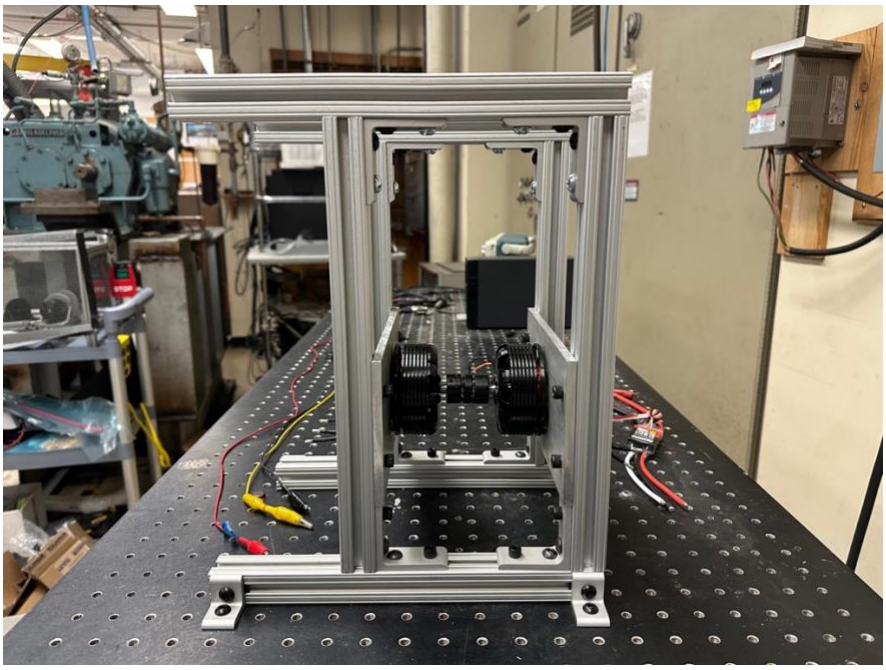

Figure 29: Assembled Dual Motor Mount with Coupling Attached

Once all connections were secured, a cage was placed over the motor mount for safety. The ESC must be armed to control the motor. To do this, the battery connection to the ESC is turned off and a 50% power signal is sent from the Arduino to the ESC. Next, the battery connection is restored, and a 0% power signal is sent to the ESC. Once the ESC gives the light and beep sequence indicating it is armed, the speed command from Simulink can be increased. By increasing the gain slider in Simulink, the motor speed changes, and the coupled motors run together. The output signal of the coupled motor can be seen in Figure 30.

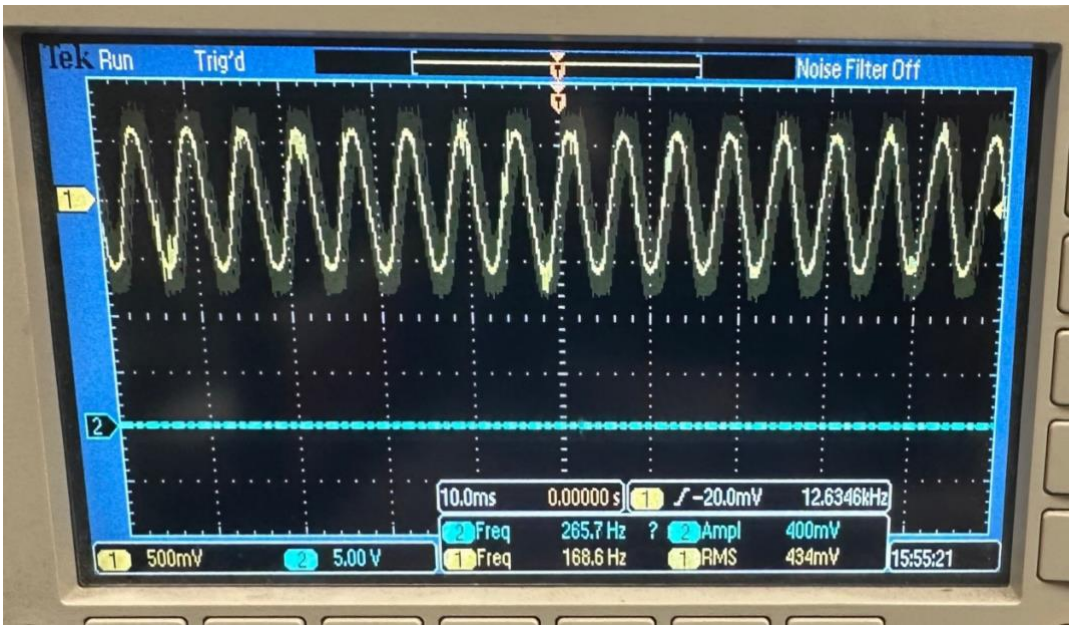

Figure 30: Output Signal of Coupled Motor

Chapter 6

Conclusion and Future Work

Summary of Work

This thesis discussed the development of a scaled hybrid electric aircraft testbed. A simulation of a possible powertrain configuration was created and tested to determine the physical parameters for the testbed. Mounts and cages were designed to assemble the testbed in an adjustable and safe manner. Finally, hardware and code were configured to allow the motor to run and be controlled by an Arduino via the serial monitor and Simulink. Implementation between the ESC, Arduino, and Simulink enables the testbed to be easily integrated with simulated components, like an engine.

The parts of the testbed designed in this thesis represent multiple parts of a more extensive testbed. A possible layout for this larger testbed can be seen in Figure 31. Boxed in green are pieces that have been developed in this thesis. The engine will be simulated using Simulink and connected to a motor pair representing the engine and generator. Other motor pairs represent the coupling of drive motors to propellors.

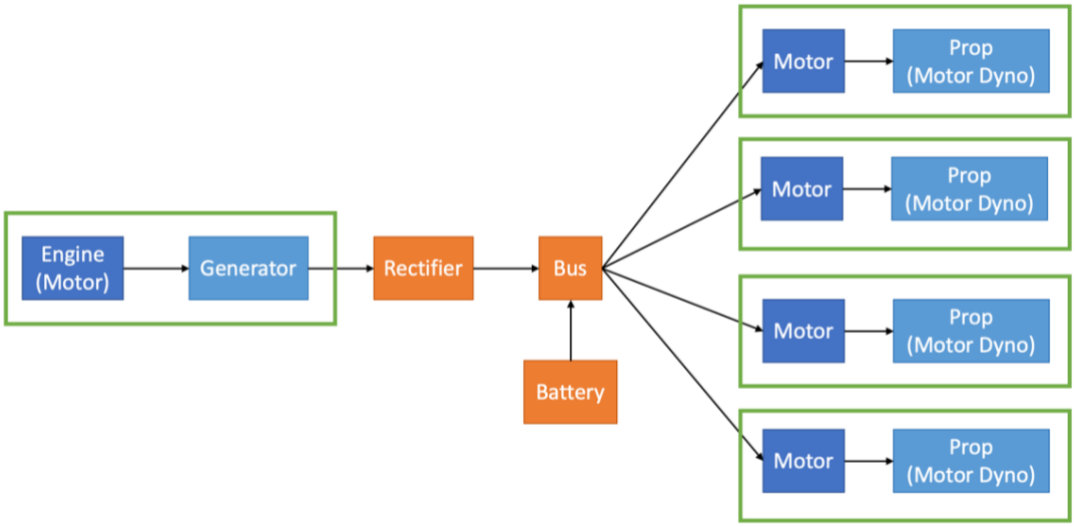

Figure 31: Designed Testbed Implementation on a Larger Scale

Ideas for Future Work

The rectifier and bus are the remaining electrical elements to be developed in the testbed. The rectifier recommended for use in the testbed is a three-phase bridge rectifier. With the dimensions and layout for the mounts and cage complete, the next step for future work would be to machine and assemble the remaining parts. The thickness of the plexiglass surrounding the testbed would need to be calculated considering the force at which parts could be ejected if a component failure occurs. The cage and the pairs of mounted motors can be assembled based on the dimensions of the engineering drawings in Appendix C.

The next step is to connect the TS106 torque transducer between the two motors. This torque transducer can measure the torque on the motor coupling and communicate this to a data acquisition system. The torque transducer will also need to be mounted higher on the testbed since the minimum height of the motor exceeds the height of the torque transducer's shaft.

Once the testbed is designed with multiple motor mount pairs and a secure cage, the next step would be to run tests to ensure that each motor pair and torque transducer interface correctly. Once the component performances have been validated, more components can be assembled following the layout in Figure 31, including a rectifier, bus, and battery.

Overall, this thesis simulated and designed an electric aircraft powertrain testbed that can be reconfigured to represent hybrid electric powertrains. The testbed was design with reconfigurability in mind and future students can develop the testbed further to result in modularity. This work builds on the literature mentioned by creating more options for aircraft testing in the design phase so that all possibilities for aircraft propulsion configurations can be analyzed and the best possibilities can be chosen for each individual mission.

Appendix A

Datasheets for Parts in Testbed

Table 5: Testbed Part List and Datasheets

Component	Manufacturer	Name
Motor	Neu Motors	6516 Link
Torque Transducer	Magtrol	TS106 torque/speed sensor Link
Shaft Coupling	Magtrol	MIC-5-0617 Link
Rectifier	Digi-Key	Bridge Rectifier Three Phase Standard 1.6 kV Chassis Mount PWS-D-Flat Link
Arduino	Arduino	Arduino Mega 2560 Link

Appendix B

Arduino Code

```
#include <Servo.h>

int potVal = 0;
int nextPotVal = 0;
byte servoPin = 9;
byte potentiometerPin = A0;
byte readsignal = A1;
int pwmSignal;
String incomingString = "";
int incomingStringInt = 0;
Servo servo;

void setup() {
  servo.attach(servoPin);
  servo.writeMicroseconds(1500);

  int PWMSignal = analogRead(A1);
  //delay(7000);
  Serial.begin(9600);
}

void loop() {
  if (Serial.available())
  {
    String incomingString = Serial.readStringUntil('\n');
    Serial.println(incomingString);

   int incomingStringInt = incomingString.toInt();
   int pwmVal = map(incomingStringInt, 0, 100, 1000, 1900);
   servo.write(pwmVal);
   //Serial.print("Potentiometer Value:");
   //Serial.println(potVal);
   Serial.print("PWM Value:");
   Serial.println(pwmVal);
   delay(500);
    }
}
```

Appendix C

Engineering Drawings of Testbed Layout

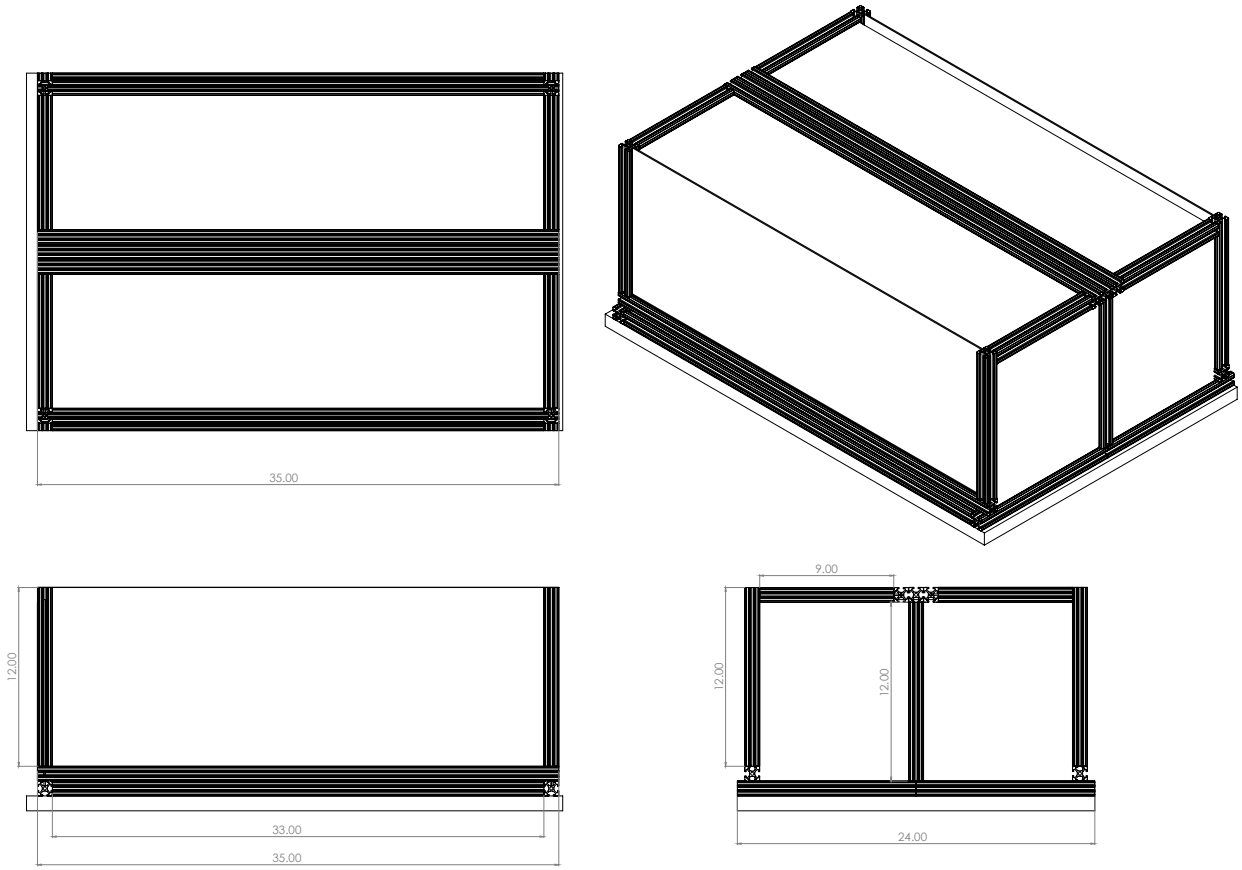

Figure 32: Testbed Cage Dimensions

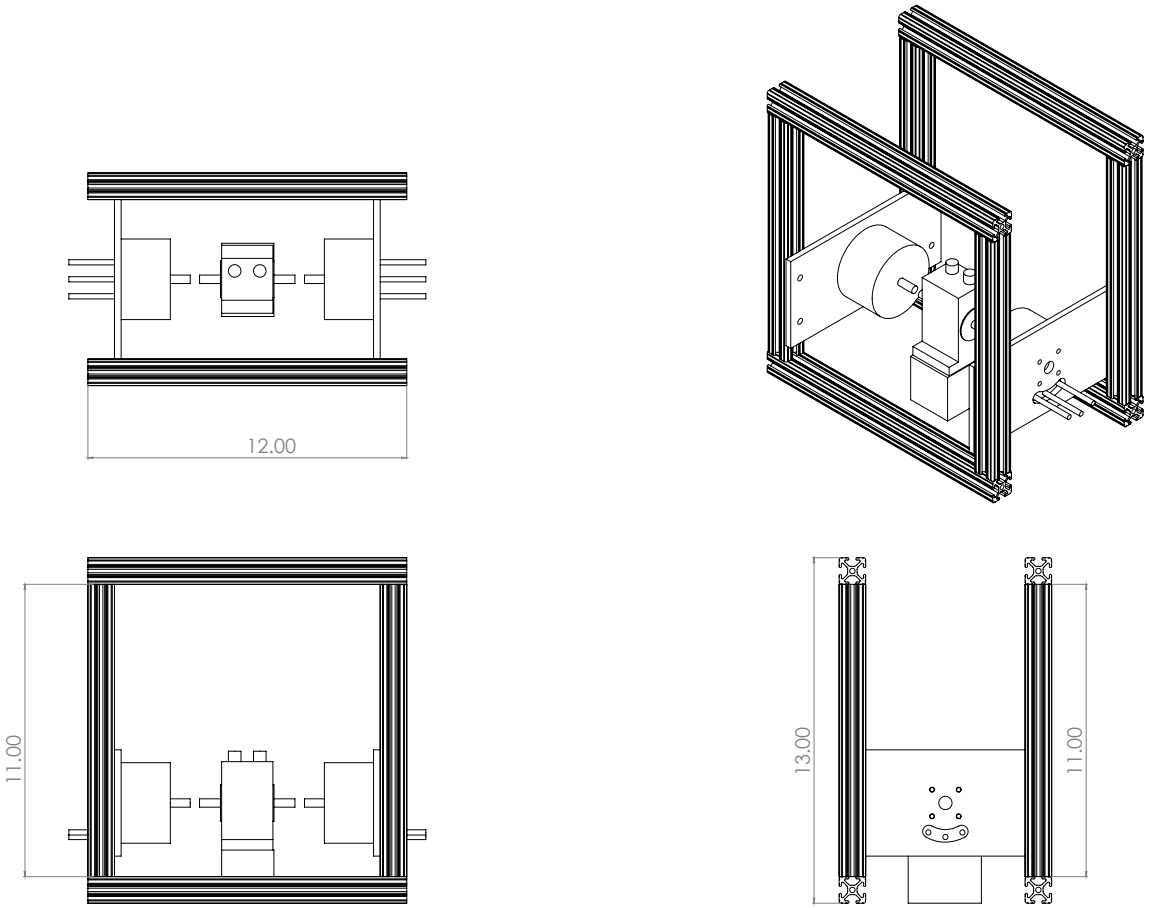

Figure 33: Dual Motor Mount Dimensions

BIBLIOGRAPHY

[1] R. W. Dyson, “Nasa electric aircraft testbed (neat) single-aisle transport air vehicle hybrid electric tail-cone thruster powertrain configuration and test results,” in *2018 AIAA/IEEE Electric Aircraft Technologies Symposium (EATS)*, IEEE, 2018, pp. 1–19. doi: 10.2514/6.2018-5004.

[2] W. Z. T. C. H. W. and D. J. Z. Huang, “Characterizing an Air-Bearing Testbed for Simulating Spacecraft Dynamics and Control,” *Aerospace*, vol. 9, no. 5, May 2022.

[3] V. Viswanathan *et al.*, “The challenges and opportunities of battery-powered flight,” *Nature*, vol. 601, no. 7894, pp. 519–525, 2022.

[4] F. G. Harmon, A. A. Frank, and J.-J. Chattot, “Conceptual design and simulation of a small hybrid-electric unmanned aerial vehicle,” *J Aircr*, vol. 43, no. 5, pp. 1490–1498, 2006.

[5] K. Milios *et al.*, “Modeling and Simulation of a Parallel Hybrid-Electric Propulsion System - Electrified Powertrain Flight Demonstration (EPFD) Program,” in *2022 IEEE Transportation Electrification Conference & Expo (ITEC)*, 2022, pp. 682–687. doi: 10.1109/ITEC53557.2022.9813981.

[6] E. and The National Academic of Sciences and Medicine, *Commercial Aircraft Propulsion and Energy Systems Research: Reducing Global Carbon Emissions*. Washington, DC: The National Academies Press, 2016. doi: 10.17226/23490.

[7] J. Rheaume and C. E. Lents, “Design and simulation of a commercial hybrid electric aircraft thermal management system,” in *2018 AIAA/IEEE Electric Aircraft Technologies Symposium*, 2018, p. 4994.

[8] S. Crow *et al.*, “Triton: A {Software-Reconfigurable} Federated Avionics Testbed,” in *12th USENIX Workshop on Cyber Security Experimentation and Test (CSET 19)*, 2019.

[9] D. K. Hall and L. F. Lollar, “Development of an Automated Electrical Power Subsystem Testbed for Large Spacecraft,” in *Proceedings of the 25th Intersociety Energy Conversion Engineering Conference*, 1990, pp. 467–470. doi: 10.1109/IECEC.1990.716939.

[10] Z. Jin, M. Ouyang, Q. Lu, and D. Gao, “Development of fuel cell hybrid powertrain research platform based on dynamic testbed,” *International Journal of Automotive Technology*, vol. 9, no. 3, pp. 365–372, 2008, doi: 10.1007/s12239-008-0044-3.

[11] B. J. Brelje and J. R. R. A. Martins, “Electric, hybrid, and turboelectric fixed-wing aircraft: A review of concepts, models, and design approaches,” *Progress in Aerospace Sciences*, vol. 104, pp. 1–19, 2019, doi: https://doi.org/10.1016/j.paerosci.2018.06.004.

[12] M.-K. Tran, M. Akinsanya, S. Panchal, R. Fraser, and M. Fowler, “Design of a hybrid electric vehicle powertrain for performance optimization considering various powertrain components and configurations,” *Vehicles*, vol. 3, no. 1, pp. 20–32, 2021, doi: 10.3390/vehicles3010002.

[13] Z. Gong *et al.*, “Design of a Reconfigurable Multi-Sensor Testbed for Autonomous Vehicles and Ground Robots,” in *2019 IEEE International Symposium on Circuits and Systems (ISCAS)*, 2019, pp. 1–5. doi: 10.1109/ISCAS.2019.8702610.

[14] C. Pinart, P. Sanz, I. Lequerica, D. García, I. Barona, and D. Sánchez-Aparisi, “DRIVE: a reconfigurable testbed for advanced vehicular services and communications.,” in *TridentCom*, Citeseer, 2008, p. 16.

[15] H. Kaisheng, J. Dinan, J. Zhenhua, and C. Linlin, “Design of Testbed System for Parallel HEV Powertrain,” in *2007 2nd IEEE Conference on Industrial Electronics and Applications*, 2007, pp. 1374–1377. doi: 10.1109/ICIEA.2007.4318631.

[16] J. Batteh *et al.*, *Development and Implementation of a Flexible Model Architecture for Hybrid-Electric Aircraft*. 2019. doi: 10.3384/ecp1815437.

[17] L. T. F. W. Silva, L. P. Resende, and M. A. Tomim, “Mathematical modeling and numerical simulation of locomotives electrical drive systems in modelica,” in *2017 Brazilian Power Electronics Conference (COBEP)*, 2017, pp. 1–8. doi: 10.1109/COBEP.2017.8257379.

[18] M. C. Knauff, C. J. Dafis, D. Niebur, H. G. Kwatny, C. O. Nwankpa, and J. Metzer, “Simulink Model for Hybrid Power System Test-bed,” in *2007 IEEE Electric Ship Technologies Symposium*, 2007, pp. 421–427. doi: 10.1109/ESTS.2007.372120.

[19] M. A. Williams, “A framework for the control of electro-thermal aircraft power systems,” University of Illinois at Urbana-Champaign, 2017.

[20] D. A. Dehesa, S. K. Menon, and M. J. Monju, “Modeling and Testing of Control Logic Approaches for Series Hybrid-Electric Powertrains for Unmanned Aerial Systems,” in *AIAA Propulsion and Energy 2020 Forum*, in AIAA Propulsion and Energy Forum. American Institute of Aeronautics and Astronautics, 2020. doi: doi:10.2514/6.2020-3961.

[21] M. Boyd, J. McNichols, M. Wolff, M. Corbett, and P. Lamm, “Effects of Transient Power Extraction on an Integrated Hardware-in-the-Loop Aircraft/Propulsion/Power System,” p. 9, Nov. 2008, doi: 10.4271/2008-01-2926.

[22] R. Roberts and D. Decker, *Energy Optimization of an Aircraft Focused on Component Sizing and Control Architecture Interactions*. 2013. doi: 10.2514/6.2013-3805.

[23] J. M. Haglage and T. W. Brown, “NASA Electric Aircraft Testbed (NEAT) Reconfiguration to Enable Altitude Testing of Megawatt-Scale Electric Machines,” in *2020 AIAA/IEEE Electric Aircraft Technologies Symposium (EATS)*, 2020, pp. 1–13.

[24] Rodger Dyson, “Hybrid Electric MC-12 Ground Testing Plan Chapter,” in *NATO Hybrid Electric MC-12 Development Plan*, NASA, 2020.

[25] S. K. Srivastava *et al.*, “A Control System Test Bed for Demonstration of Distributed Computational Intelligence Applied to Reconfiguring Heterogeneous Systems,” in *2007 1st Annual IEEE Systems Conference*, 2007, pp. 1–8. doi: 10.1109/SYSTEMS.2007.374668.

[26] A. Rangesh, K. Yuen, R. K. Satzoda, R. N. Rajaram, P. Gunaratne, and M. M. Trivedi, “A Multimodal, Full-Surround Vehicular Testbed for Naturalistic Studies and Benchmarking: Design, Calibration and Deployment,” *arXiv e-prints*, 2019.

[27] B. Yang, L. Guo, and J. Ye, “Real-time Simulation of Electric Vehicle Powertrain: Hardware-in-the-Loop (HIL) Testbed for Cyber-Physical Security,” in *2020 IEEE Transportation Electrification Conference & Expo (ITEC)*, 2020, pp. 63–68. doi: 10.1109/ITEC48692.2020.9161525.

[28] S. Thanagasundram, R. Mcmurran, A. Mouzakitis, C. Matthews, and R. P. Jones, “Reconfigurable Hardware-in-the-Loop Simulator,” *Journal of the Institute of Measurement and Control*, vol. 43, pp. 273–277, Nov. 2010, doi: 10.1177/002029401004300902.

[29] K. Pieper, A. Perry, P. Ansell, and T. Bretl, “Design and Development of a Dynamically, Scaled Distributed Electric Propulsion Aircraft Testbed,” in *2018 AIAA/IEEE Electric Aircraft Technologies Symposium (EATS)*, IEEE, 2018, pp. 1–2. doi: 10.2514/6.2018-4996.

[30] C. T. Aksland, “Modular modeling and control of a hybrid unmanned aerial vehicle’s powertrain,” 2019.

[31] C. T. Aksland and A. G. Alleyne, “Experimental Model and Controller Validation for a Series Hybrid Unmanned Aerial Vehicle,” in *2020 American Control Conference (ACC)*, 2020, pp. 4154–4160. doi: 10.23919/ACC45564.2020.9147529.

[32] O. Pfeifle *et al.*, “Distributed Electric Propulsion for Yaw Control: Testbeds, Control Approach, and Flight Testing,” in *AIAA AVIATION 2021 FORUM*, in AIAA AVIATION Forum. American Institute of Aeronautics and Astronautics, 2021. doi: doi:10.2514/6.2021-3192.

[33] E. A. Baumann, J. Hernandez, and J. Ruhf, “An Overview of NASA’s SubsoniC Research Aircraft Testbed (SCRAT),” in *AIAA Atmospheric Flight Mechanics (AFM) Conference*, in Guidance, Navigation, and Control and Co-located Conferences. American Institute of Aeronautics and Astronautics, 2013. doi: doi:10.2514/6.2013-5083.

[34] T. Jordan, W. Langford, and J. Hill, “Airborne Subscale Transport Aircraft Research Testbed - Aircraft Model Development,” in *AIAA Guidance, Navigation, and Control Conference and*

Exhibit, in Guidance, Navigation, and Control and Co-located Conferences. American Institute of Aeronautics and Astronautics, 2005. doi: doi:10.2514/6.2005-6432.

[35] Michael Kerho, "Turboelectric Distributed Propulsion Test Bed Aircraft," El Segundo, 2015.

[36] K. C. Pieper, "Design, development and evaluation of a distributed electric propulsion testbed aircraft," University of Illinois at Urbana-Champaign, 2018.

[37] T. Joels, N. Yechieli, L. Edery-Azulay, and D. E. Raveh, "Design, Analyses, and Flutter Testing of the Active Aeroelastic Aircraft Testbed (A3TB) Platform," in *AIAA SCITECH 2022 Forum*, in AIAA SciTech Forum. American Institute of Aeronautics and Astronautics, 2021. doi: doi:10.2514/6.2022-2419.

[38] P. G. Hamel, "5.4.2 Beagle Bassett VSS (1973–2014)," in *In-Flight Simulators and Fly-by-Wire/Light Demonstrators A Historical Account of International Aeronautical Research*, 2017, pp. 63–64.

[39] Dalton Decerio, "Benefits of Parallel Hybrid Electric Propulsion for Aircraft and Rotorcraft," The Pennsylvania University, 2022.

[40] James Bennink, "Modeling Gas Turbine Dynamics for a Hybrid-Electric Propulsion System Simulation," The Pennsylvania State University, 2022.

ACADEMIC VITA

Carly Dunford
cnd5216@psu.edu

EDUCATION:

The Pennsylvania State University, University Park, PA **Aug. 2019 – May 2023**
Schreyer Honors College
Bachelor of Science in Mechanical Engineering, Mechatronics Minor

WORK EXPERIENCE:

Boeing Space – Phantom Works, Kent, WA **June 2022– Aug. 2022**
Mechanical Engineering Intern

- Developed a MATLAB tool that tracked given points in a video and calculated linear velocity, angular velocity, and trajectory of an object to be used in a test to determine these parameters for a satellite launched from a capsule in space.
- Assembled a glass transportation system utilizing pressurized air and suction cups to transport 0.001-inch-thick glass safely and efficiently.
- Modeled a silver bullet transportation system in CATIA to transport multiple classified objects between closed areas safely and securely.

Collins Aerospace, Vergennes, VT **May 2021– Aug. 2021**
Quality Assurance Engineering Intern

- Led the effort to verify that all non-conforming material areas in the plant were correct according to work instructions and corrected discrepancies before an AS9100 recertification audit.
- Assisted in reconstructing the quality issue management system to improve the closure of quality investigations after receiving a corrective action report for overdue investigations.
- Conducted containment on high-frequency accelerometers, integrated vehicle health management units (IVHMUs), and the reliability-enhanced stabilator actuator (RESA) to prevent escapes and allow the company to ship products on time to meet monthly and quarterly goals.

Piasecki Aircraft Corporation, Essington, PA **Summers 2017-2020**
Engineering Intern

- Modeled helicopter cyclic control system parts in SolidWorks for a kinematic study which eventually will be manufactured at a leading helicopter company.
- Calculated and compared weights on different aircraft configurations to add to a proposal for the US Army.
- Developed a heat load model for new electric aircraft and contacted a major U.S. aircraft air conditioning supplier, which resulted in a request for proposal.
- Reconstructed an aircraft cost model for electric vertical takeoff and landing helicopters
- Delineated US Army customer requirements into a database to track proposal timeline adherence.

SOFTWARE:

SolidWorks, Catia, Microsoft Office, SAP Enterprise Resource Planning Software, MATLAB, Final Cut Pro

LEADERSHIP & INVOLVEMENT:

Advanced Controls Lab Research Assistant	Present
Phi Sigma Rho Engineering Sorority	2021- Present
- Alumni Relations Chair	2021
Member, Vertical Flight Society, Penn State Chapter	Present
CAD Teaching Assistant for Engineering Design	2020
Member, Society of Women Engineers	2019-Present